Dual control of external surface and internal pore structure of small ordered mesoporous silica particles directed by mixed polyion complex micelles

Jason Richard, Anthony Phimphachanh, Alix Jamet-Fournier, Thomas Cacciaguerra, Philippe Dieudonné-George, Didier Cot, Mathias Destarac, Patrick Lacroix-Desmazes, Martin In, Nathalie Marcotte, et al.

To cite this version:

Jason Richard, Anthony Phimphachanh, Alix Jamet-Fournier, Thomas Cacciaguerra, Philippe Dieudonné-George, et al.. Dual control of external surface and internal pore structure of small ordered mesoporous silica particles directed by mixed polyion complex micelles. Microporous and Mesoporous Materials, 2022, 338, pp.111915. 10.1016/j.micromeso.2022.111915 . hal-03867129

HAL Id: hal-03867129
https://hal.science/hal-03867129v1

Submitted on 23 Nov 2022

Dual control of external surface and internal pore structure of small ordered mesoporous silica particles directed by mixed polyion complex micelles

Jason Richard,[a] Anthony Phimphachanh,[a,b] Alix Jamet-Fournier,[a] Thomas Cacciaguerra,[a] Philippe Dieudonné-George,[b] Didier Cot,[c] Mathias Destarac,[d] Patrick Lacroix-Desmazes,[a] Martin In,[b] Nathalie Marcotte[a] and Corine Gérardin*[a]*

[a] Institut Charles Gerhardt, Univ Montpellier, CNRS, ENSCM, Montpellier, France

[b] Laboratoire Charles Coulomb, Univ Montpellier, CNRS, Montpellier, France

[c] Institut Européen des Membranes, Univ Montpellier, CNRS, ENSCM, Montpellier, France

[d] IMRCP, Université Toulouse III, CNRS, Toulouse, France

Abstract

A versatile approach has been developed to prepare small mesoporous silica particles with simultaneous control of the internal ordered pore structure and the external particle surface. Mixed polyion complex (PIC) micelles are used as silica structure-directing agents: they result from the complexation of a polybase with two polyacid double-hydrophilic block copolymers (DHBC) having either a poly(ethylene oxide) (PEO) based-block or a polyacrylamide (PAM) block. The ionizable block in both DHBC is poly(acrylic acid), which complexes oligochitosan to form the core of the electrostatic complex. By varying the architecture of the PEO-based block (linear or comb-shaped) and the synthesis parameters, it is possible to modulate the pore structure from 3D cage-like to 2D-hexagonal and lamellar mesostructures. Replacing a fraction of the PEO-based polymers with DHBC having a polyacrylamide block that has no affinity for silica is shown to affect silica-micelle interactions and material growth. While the PEO chains interact with silica to form the hybrid interface, the PAM chains act as capping agents and control the external surface of the particles. Increasing the relative amount of PAM-based DHBC leads to the formation of small discrete mesoporous silica particles that are reduced in size to 200 nm. The particle size reduction and particle surface stabilization by PAM chains can be explained by considering not only the existence of a mixed corona of PAM and PEO in PIC micelles but also the differentiated solubility of these two neutral blocks induced by silica condensation. Thus, the present strategy allows independent decrease of the particle size and tuning of its pore structure.

KEYWORDS: mesoporous materials • particles • polyion complex micelles • mesostructure control • double-hydrophilic block copolymer • hybrid organic–inorganic interface

Introduction

The discovery of ordered mesoporous silica materials in the early 1990s and their remarkable potential applications for adsorption, catalysis, sensing and drug delivery systems [1–4] stimulated researchers' enthusiasm to better control their unique properties such as high surface areas, tunable pore sizes and shapes, mesostructure diversity and controlled morphologies. Designing small and regular sub-micrometer size particles gives mesoporous materials higher performance due to better accessibility of the mesopores, improved mass transfer in the pores and homogeneous dispersion of the particles in matrices.

Several synthetic approaches have been developed to reduce the size of structured silica mesoporous particles, as recently reported in several reviews.[5–9] They all rely on a delicate control of the hydrolysis and condensation rates of the silicon alkoxide in the synthesis medium to balance the two fundamental processes required for the formation of ordered mesostructured nanomaterials: the mesophase structuring by the cooperative organization of the template and the inorganic precursor, and the growth of the organic/inorganic assembly. This is usually achieved by controlling the processing pH parameter using various types of acid or base, introducing additives such as alcohols and inorganic salts, and varying the template and the inorganic sources. Strategies based on high dilution methods involving cationic surfactants in alkaline media,[10–15] which avoid particle aggregation and can be further improved by quenching procedures,[16] growth and aggregation inhibition approaches using organic amines [17,18] or dual surfactant systems,[19–21] and the spray-drying process [22] are of particular interest to easily synthesize monodisperse meso-ordered nanoparticles. However they all operate under particularly difficult synthesis conditions, using either a strong basic medium [10,11,23,12–19] or a strong acidic medium [20–22,24,25]. These synthesis conditions do not correspond at all to the current societal demand for more sustainable industrial processes. It should be mentioned that only a few studies have reported the preparation of monodisperse mesoporous silica nanoparticles at near neutral pH, all of them employing the small pore-forming cationic cetyltrimethylammonium halide surfactant (CTA).[26,27] In the presence of various additives (alcohols, amines, inorganic bases and inorganic salts) affecting the hydrolysis and condensation processes of silica species, Qiao et al.[26] highlighted the crucial role of the initial pH of the synthesis medium in controlling the size of nanoparticles. In their study, the use of inorganic buffer salts allowed the nanoparticle size to vary from 30 nm at pH 9 to 85 nm at pH 6. However, the spherical nanoparticles exhibited a disordered pore network of wormlike topology. Using different CTA counterions and low concentration of small organic amines, Zhang et al. [27] also obtained monodisperse non-ordered mesoporous nanoparticles with stellate or raspberry channel morphology, which were however produced at the kilogram-scale. Thus, there is still a need to eco-design well-dispersed submicronic particles with large pore diameter and homogeneous ordered porous structure.

A decade ago, we proposed a novel structure-directing agent, namely a polyion complex (PIC) assembly stabilized by a neutral poly(ethylene oxide) (PEO) corona, to prepare ordered silica-based structures in water under slightly acidic to neutral pH conditions.[28] The macroscopic precipitation of the mesostructured hybrid organic/inorganic material is fast, operates at room temperature and does not require hydrothermal treatment. It originates from a hydrogen bonding interaction between silicic species (Si) and ether oxygen of the neutral PEO block of a double hydrophilic block copolymer (DHBC) with a weak polyacid as a second block. The polyacid block, usually poly(acrylic acid) (PAA) or poly(methacrylic acid) (PMAA), is meanwhile involved in the electrostatic complexation of a weak polyamine, such as oligochitosan (OC),[29,30] poly-*L*-lysine [31–33] or aminoglycoside antibiotics,[34–36] forming an organic complex coacervate core which then produces the mesoporous network after calcination of the material. Various topologies (cylindrical hexagonal, lamellar, wormlike) of the PIC-templated mesostructured materials (hereafter referred to as the mesoPIC family of materials) were obtained by simultaneously controlling the relative extents of hydrogen bonding interaction of the silicic species with the EO units, the electrostatic complexation of the polyions between the carboxylate (AA) and amine (N) groups, and the silica condensation rate. Control of the structure was achieved by fine-tuning the synthesis conditions of the material, including the N/AA ratio of complexation units, the ratio of ethylene oxide units to silicon species, the overall mass concentration of the synthesis medium[30] and its pH.[31]

While our previous studies have established the interplay between the mesoscopic scale order of materials and the interactions between the different constituents of the system, little is yet known about the morphological control of mesoPIC materials. We only noticed the possibility of reducing the particle size by increasing the pH of the synthesis medium,[30] which accelerates the rate of polycondensation of silicic species as already established when using other structure-directing agents composed of polyethylene oxide.[37,38] In fact, the

2300 nm size spherical particles obtained at pH = 4.5 using PEO-*b*-PAA/oligochitosan as PIC template of silica decreased to an average size of about 220 nm at pH = 7.9, while appearing highly polydispersed in size and agglomerated. Despite a decrease in particle size, the change in pH of the synthesis medium also inevitably disrupts the interactions between the different constituents of the system (EO with Si, AA with N), deteriorating the quality of the long-range structural order. Therefore, reducing the size of the particles independently of their structural and porous properties would provide an attractive method to prepare ordered mesoporous materials with tunable pore arrangement and diameter under environmentally friendly conditions.

In this work, we intend to reduce the size of mesoporous silica particles, while controlling the mesoscopic structural order by using an original PIC-templated strategy in a sustainable one-pot process. It relies on the use of an additional DHBC, namely a poly(acrylamide)-*b*-poly(acrylic acid) (PAM-*b*-PAA) that will act as a particle size regulator, in addition to PEO-*b*-PAA/oligochitosan PIC micelles that we classically use to control the internal porous structure of the silica particles. We postulate that the PAM block with lower affinity than PEO for silica and high water solubility should promote control of the particle external surface and steric stabilization of the particles in water, while the PAA block of the PAM-*b*-PAA should provide anchoring of the polymer into the hybrid mesoPIC material (through the core of the PIC micelle). The choice of this additional DHBC was also guided by its successful use as a capping agent in the preparation of sterically stabilized nanoparticles of high colloidal stability and controlled size of metal hydroxide, metal sulfide and layered double hydroxide phases in aqueous media.[39–41] The ability to synthesize PEO-based DHBC polymers with controlled architecture and block molecular weights was exploited to prepare materials with three different ordered pore structures. In particular, the specific characteristics of the comb-type poly((ethylene oxide) methylether acrylate)-*b*-poly(acrylic acid) (PAPEO-*b*-PAA) copolymer compared to its linear counterpart of the same molecular weight (PEO-*b*-PAA) have been used to extend the range of available mesoPIC materials to ordered cage-like structures.

Results and Discussion

First, ordered mesoporous silica materials templated by PIC were prepared using only the PEO-based diblock copolymer with oligochitosan (OC) to structure silica. Their synthesis consisted of a two-step one-pot approach. First, the reactants (tetraethoxysilane TEOS, PEO-*b*-PAA or PAPEO-*b*-PAA of Fig. 1 and OC) were mixed together in an acidic aqueous solution at pH = 2 to hydrolyze the silica precursor. Second, the pH was increased to 4.5 to promote macroscopic precipitation from the simultaneous formation of polyion complex (PIC) and condensation of silica oligomers. It resulted in the formation of two well-defined ordered mesostructures exhibiting an organization that depends on the configuration of the PEO-based block: a 2D hexagonal structure (**HEX-0**) having cylindrical pores (P6mm) when using the linear PEO-*b*-PAA copolymer, and a cubic structure (**CUB-0**) possessing interconnected cage-like pores when using the comb-type PAPEO-*b*-PAA. Evidence for the long-range ordering of the mesostructures is given by TEM images (Fig. 1) and SAXS profiles (Fig. 2c and 2d) of the calcined materials. The latter shows up to five distinct scattering peaks at low q values (0.38, 0.66, 0.75, 1.00 and 1.13 nm^{-1}) assigned to the (100), (110), (200), (210) and (300) diffraction planes for **HEX-0**, and three at q = 0.65, 1.04 and 1.20 nm^{-1} for **CUB-0** suggesting a cubic Fd3m or Fm3m type structure. It should be noted that the TEM images of **CUB-0** appear to highlight some domains of quasi-crystalline structure that merit further investigation. Structural mesoporosity is revealed by the typical type-IV shape of the N_2 sorption isotherms of **HEX-0** and **CUB-0** exhibiting H1 and H2-type hysteresis loops (Fig. 2a and 2b), respectively. Large mesopore diameters of up to 10 nm for **HEX-0** and 6.2 nm for **CUB-0** were determined from the narrow pore size distributions (PSDs) obtained from the adsorption branch by the NLDFT method (Fig. S1b).[42] The smaller mesopore volume of **HEX-0** (0.30 $cm^3.g^{-1}$) compared to that of **CUB-0** (0.55 $cm^3.g^{-1}$) stems from the greater silica wall thickness in **HEX-0** (9.1 nm) compared to that of **CUB-0** (2.0 nm, see Fig. 2e and Table S1a). The smaller mesopore volume of **HEX-0** is consistent with the lower organic content (51 wt.% *vs.* 57 wt.% for **CUB-0**) of the corresponding as-synthesized mesoPIC hybrid material as determined by TGA. The difference in structure could not be related to a difference in chemical composition of the materials, as revealed by the similarity in silica yield (90 wt.%) and polyion ratio (N/AA=0.50, where N is the number of amino functions in OC and AA is the number of carboxylic acid function in the copolymer), but rather to a difference in the morphologies of PIC mesophases. While the **HEX-0** mesostructure is templated by cylindrical PIC assemblies, **CUB-0** is templated by cage-like assemblies. These morphological differences are in good agreement with the differences in the length of the neutral copolymer block backbone, which is shorter for the comb PAPEO architecture (DP(PAPEO)=20) than for the linear PEO counterpart of similar molecular weight (DP(PEO)=227). This smaller length of the comb PAPEO block of similar molecular weight leads to an increase in the interfacial curvature between the soluble corona and insoluble coacervate core (PAA/OC) of the assembly that further defines the type of mesostructure.[43–46] From a theoretical perspective, the difference in mesostructures (**HEX** or **CUB)** obtained here correlates well with the shift (2D HEX to CUB) predicted in order-to-order transitions in diblock copolymer melts in the case of smaller conformational asymmetry, as examined by Matsen and Bates.[47]

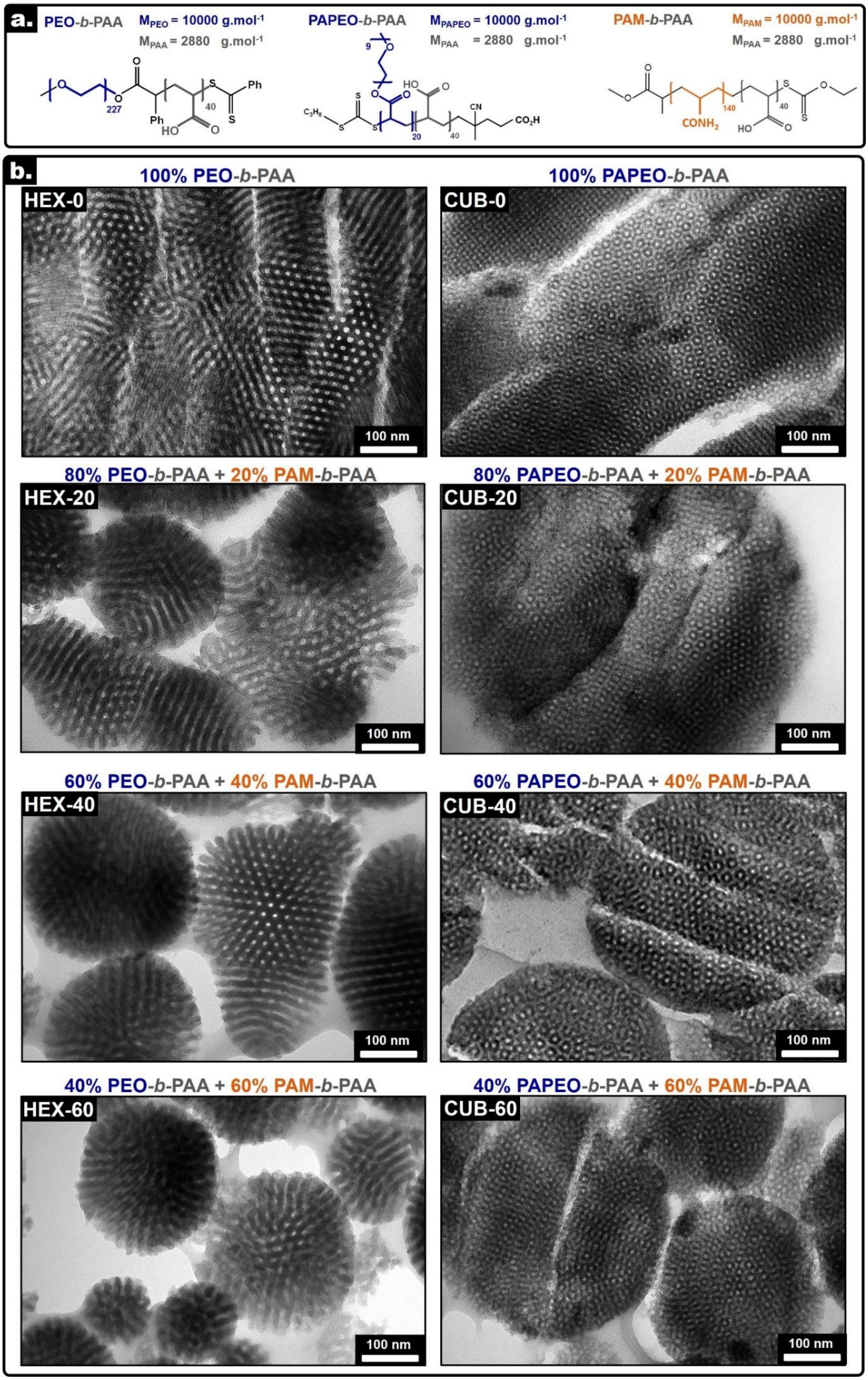
a.
PEO-b-PAA
M_PEO = 10000 g.mol-1
M_PAA = 2880 g.mol-1
227
40
Ph
Ph
HO
O
S
S
PAPEO-b-PAA
M_PAPEO = 10000 g.mol-1
M_PAA = 2880 g.mol-1
9
20
40
CN
CO2H
C3H8
PAM-b-PAA
M_PAM = 10000 g.mol-1
M_PAA = 2880 g.mol-1
140
40
CONH2
b.
100% PEO-b-PAA
HEX-0
100% PAPEO-b-PAA
CUB-0
80% PEO-b-PAA + 20% PAM-b-PAA
HEX-20
80% PAPEO-b-PAA + 20% PAM-b-PAA
CUB-20
60% PEO-b-PAA + 40% PAM-b-PAA
HEX-40
60% PAPEO-b-PAA + 40% PAM-b-PAA
CUB-40
40% PEO-b-PAA + 60% PAM-b-PAA
HEX-60
40% PAPEO-b-PAA + 60% PAM-b-PAA
CUB-60
100 nm

Figure 1. Formula of the different DHBC used (a) and TEM images of calcined microtome-cut particles (b). The ratio of DHBC used in each material synthesis is indicated above the corresponding image.

In the absence of PAM-*b*-PAA, materials are macroscopic and cover the entire field of SEM micrographs (Fig. 3a). The particle shape is irregular and their size polydisperse. On the other hand, replacing a fraction of the PEO-based DHBC with PAM-*b*-PAA, of the same block molecular weights, leads to dispersed particles of homogeneous morphology and whose sizes are considerably reduced compared to the reference materials. Increasing the proportion of PAM-*b*-PAA to 60% of the DHBCs while adjusting the concentration of TEOS to keep EO/Si constant, allows reducing the particle size to 220 nm for **HEX-60** and 350 nm for **CUB-60** while preserving their original ordered structure (Table 1). This unambiguously demonstrates that using a mixture of (PA)PEO-*b*-PAA and PAM-*b*-PAA copolymers allows obtaining well-dispersed particles of controlled morphology and reduced size. The microtome cutting process perfectly reveals the internal pore structure and structural order in the particle volume. But it should be noted that it results in images of particle cross sections made randomly throughout the particle volume, which inherently leads to images with overestimated apparent polydispersity of particle diameters. It also leads to slightly underestimated particle diameters, but nevertheless clearly shows the decrease in particle size when increasing the fraction of PAM-based DHBC. Interestingly, the hydrodynamic diameters measured by DLS on **HEX** hybrid particles redispersed in aqueous solution and the diameter of the calcined particles determined from TEM images have similar values (d_{DLS}/d_{TEM} ratio typically below 1.3), highlighting the possibility of redispersing the hybrid particles in water after centrifugation without aggregation phenomenon.

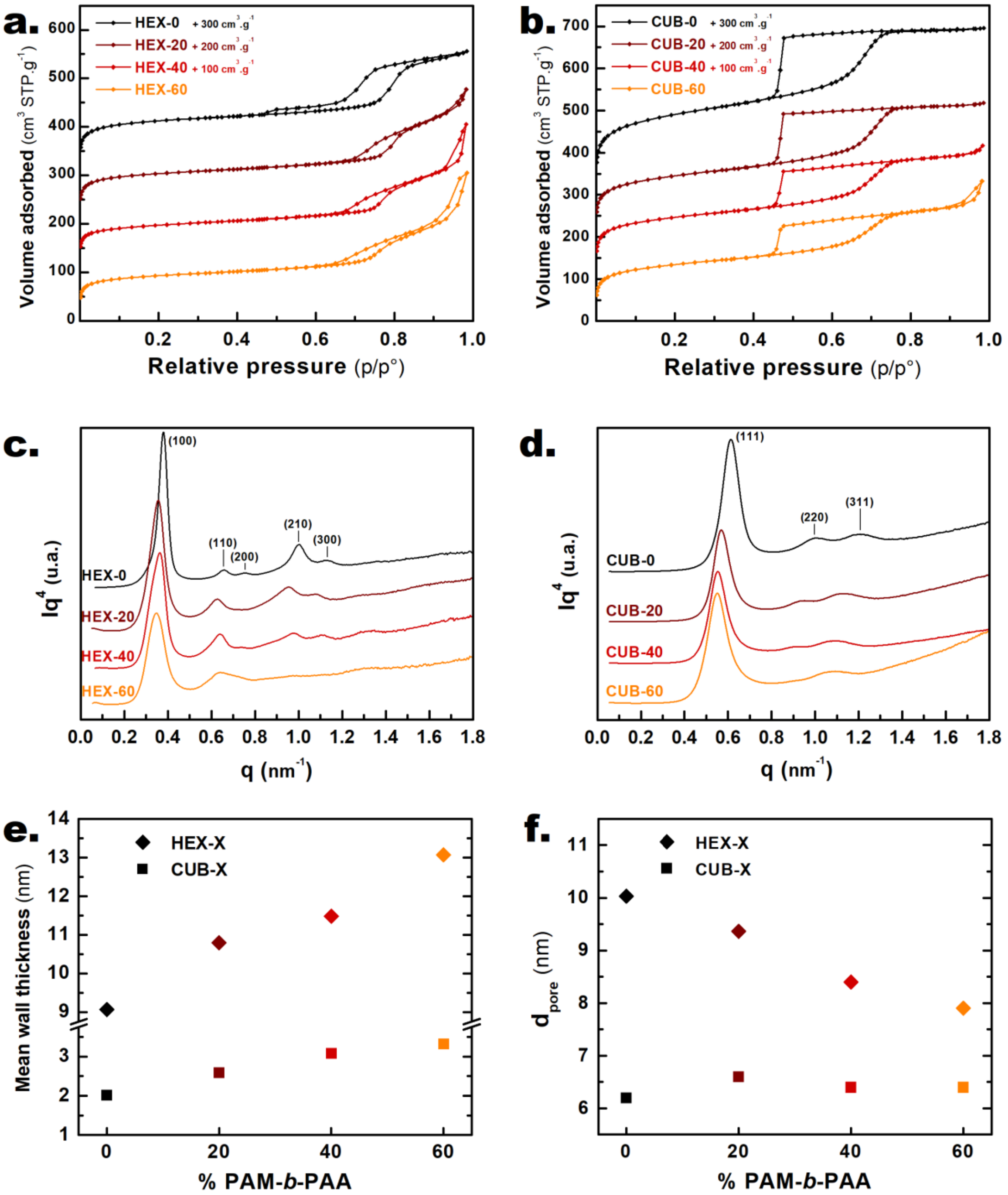

Figure 2. Porous properties of the calcined particles: N2 sorption isotherms of HEX (a) and CUB (b) particles, SAXS patterns of calcined HEX (c) and CUB (d) particles. Evolution of mean wall thickness (e) and mean mesopore diameter (f) with %PAM-*b*-PAA. Isotherms are shifted by 100 cm^3.g^{-1} relative to each other from HEX-60 and CUB-60 for clarity.

Regardless of the fraction of PAM-*b*-PAA, the ordered hexagonal and cubic mesostructures of the materials are remarkably preserved, as illustrated by the TEM images in Fig. 1b. All **HEX** and **CUB** materials show easily distinguishable intense SAXS diffraction peaks, confirming the long-range ordering and type of the mesostructures (Fig. 2c and Fig. 2d). The coherence length (*L*, Table S1a), calculated from the Debye-Scherrer equation, remains high and almost constant (*i.e.* 73 ± 9 nm for hexagonal and 63 ± 6 nm for cubic particles) with decreasing particle size, meaning that the particles are still long range ordered regardless of the amount of PAM-*b*-PAA used.

Table 1. Diameters of particles synthesized in the presence of PAM-*b*-PAA.

Particle diameter (nm)	HEX-20	HEX-40	HEX-60	CUB-20	CUB-40	CUB-60
d_{DLS} [a]	390	310	180	N/A	N/A	N/A
d_{TEM} [b]	309	302	228	> 1000	542	354
σ_{TEM} [c]	86	70	57	N/A	108	120

[a] diameter determined from DLS experiment (d_{DLS}) on hybrid particles dispersed in aqueous solution (colloidal stability of CUB particles in aqueous solution was not sufficient to measure their hydrodynamic diameter), [b] diameter determined from TEM images (d_{TEM}) on calcined particles, [c] standard deviation.

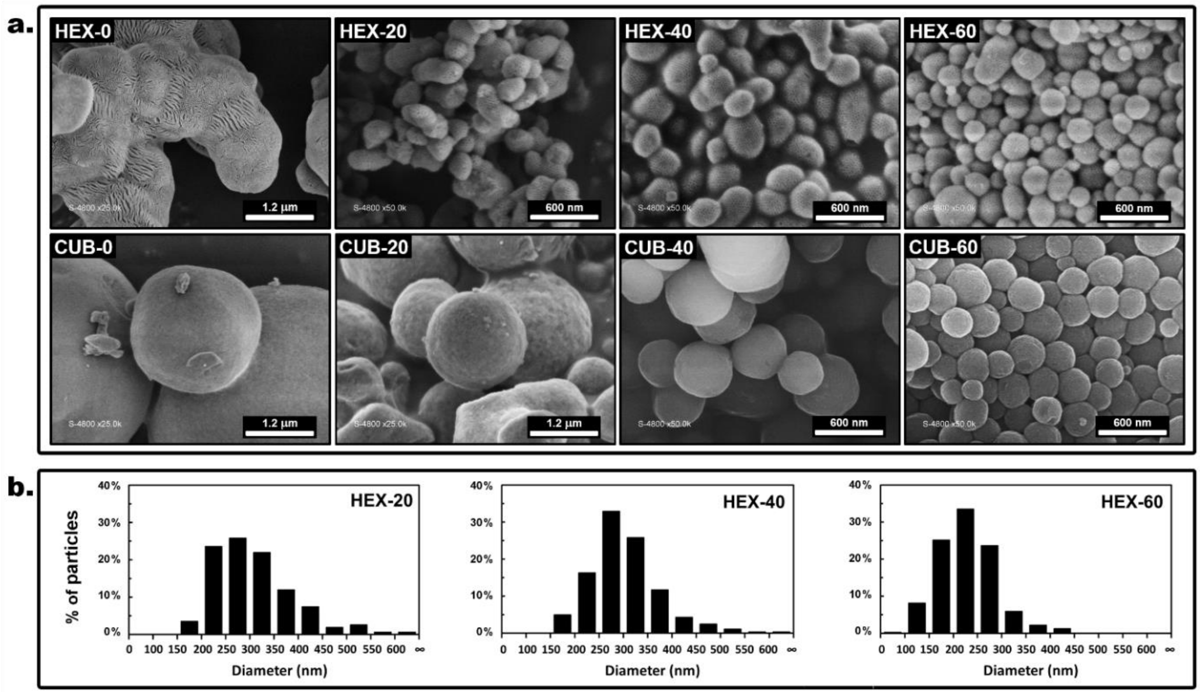

Figure 3. a) SEM images of HEX (1st row) and CUB (2nd row) mesoPIC hybrid particles obtained by introducing 0, 20, 40 and 60 % of PAM-*b*-PAA in the synthesis medium. b) analysis of the size distribution of calcined HEX material from TEM images.

The decrease in particle size is also observed in the adsorption isotherms (Fig. 2a and Fig. 2b). The interparticle porosity revealed at $p/p^0 > 0.85$ increases when the fraction of PAM-*b*-PAA increases. All other textural features calculated from the nitrogen sorption measurements, such as mesoporous (V_{meso}) and microporous (V_{micro}) volumes, mesopore diameter (d_{pore}) and mean wall thickness (h_{mean}) are shown in Table S1a. The main feature is the decrease in V_{meso} as the %PAM-*b*-PAA increases for **HEX** and **CUB** materials while the value of *d*-spacing corresponding to the first pseudo-Bragg peak (d_0) remains almost constant. For the hexagonal materials, the decrease in V_{meso} correlates with both a decrease in mesopore diameter (from 10.0 nm for **HEX-0** to 7.9 nm for **HEX-60**, Fig. 2f and PSDs in Fig. S2b) and an increase in silica wall thickness (from 9.1 nm for **HEX-0** to 13.1 nm for **HEX-60**, Fig.2e). In contrast, the change in mesoporous volume of the cubic materials is explained only by an increase in silica wall thickness (from 2.0 nm for **CUB-0** to 3.3 nm for **CUB-60**, Fig. 2e).

Surprisingly, the TGA results on the particles show that the organic content is independent of the initial amount of PAM (Table S1b). Furthermore, PAM-*b*-PAA could not be detected specifically in the mesoPIC particles neither by ^{13}C (Fig. S2a) and ^{15}N (Fig. S2b) NMR, nor by FTIR spectroscopy (Fig. S3). Despite the lack of a clear signature, the crucial role of PAM-*b*-PAA in decreasing particle size still suggests it might be present, if not inside the particles, at least on their surfaces. This would be consistent with a small amount of PAM-*b*-PAA in the hybrid particles that could not be detected using conventional characterization methods of bulk materials. Thus, by using XPS spectroscopy to probe the particle surface, we were able to identify the presence of PAM-*b*-PAA. The N_{1S} XPS spectra of hybrid mesoPIC particles synthesized in the absence of PAM-*b*-PAA (**HEX-0** and **CUB-0**) and in the presence of PAM-*b*-PAA (**HEX-60** and **CUB-60**) are shown in Fig. 4 for the **HEX** materials and Fig. S4a for the **CUB** series. **HEX-0** (Fig. 4, left) shows two bands of approximately similar area peaking at 399.5 and 401.8 eV (Table S4) and attributed to the NH_2 and NH_3^+ functions of oligochitosan (Fig. S4b), respectively.[48,49] The N_{1S} XPS spectrum of **HEX-60** (Fig. 4, right) differs by an increased intensity of the highest energy band, which is related to the presence of NH-C=O group of PAM-*b*-PAA (Fig. 4, middle). This clearly shows the presence of PAM-*b*-PAA on the outer surface of mesoPIC small particles. Similar features were observed for **CUB-60** (Fig. S4a), except that the amount of PAM-*b*-PAA was found to be lower than that of **HEX-60** particles (11 % nitrogen atoms instead of 35 %, Table S4).

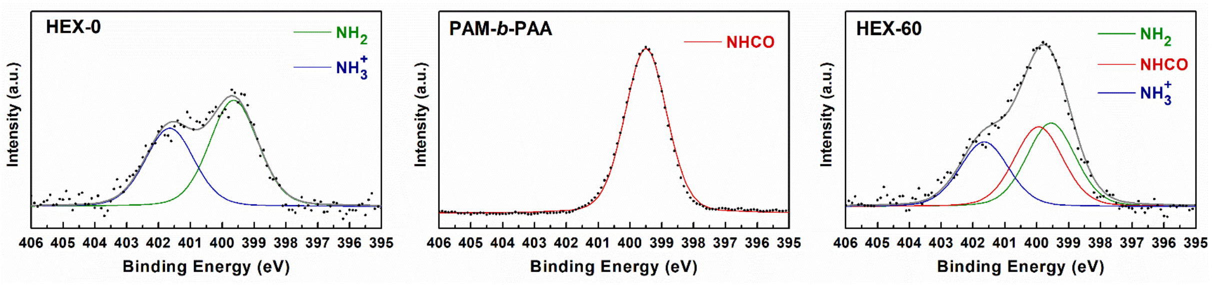

Figure 4. N1s XPS spectra of HEX-0 material (left), PAM-*b*-PAA polymer (middle) and HEX-60 material (right).

All these results lead us to propose a mechanism for the size decrease of mesoPIC particles, which is based on the role of PAM-*b*-PAA polymers as capping agents controlling and stabilizing the external surface of particles. The first event for the formation of well-defined mesostructures is the creation of an organic-inorganic hybrid interface between the PIC assemblies and the hydrolyzed silicic species, which is driven by hydrogen bonding involving ether oxygen (EO) as is the case for some classical poly(ethylene oxide) based structure-directing agents.[50,51] The second key fact to control the mesostructure is the need to govern the organic-inorganic interfacial curvature by tuning the relative sizes of the electrostatic complex core (PAA/OC coacervate) and the (PA)PEO/inorganic corona. In the present study, ordered structuring of silica was achieved not only by using the (PA)PEO-*b*-PAA copolymer alone as has been successfully experimented before,[28,30,52] but also by replacing part of it with various amounts of PAM-*b*-PAA. The resulting PIC assembly from these mixtures is expected to be composed of an electrostatic core formed by complexation between the oligochitosan and PAA blocks of the two copolymers, and a corona of mixed PAM/(PA)PEO blocks. Indeed, miscible binary blends have been reported to form through hydrogen bonds between the amide and ether groups in concentrated aqueous solutions of low molecular weight PAM and PEO polymers.[53–55] Here, varying the amount of PAM-*b*-PAA allows the composition of the corona to be adjusted while keeping the core composition unchanged. The role of PAM-*b*-PAA in reducing the particle size while keeping their mesostructure unchanged then obviously holds from the corona whose PAM content increases. Moreover, all attempts to structure silica with pure PAM-*b*-PAA based micelles have failed: the absence of (PA)PEO-*b*-PAA leads to gelation rather than macroscopic precipitation of the hybrid material. This highlights the low affinity of silicic species for the PAM block of PAM-*b*-PAA compared to the PEO block. This is in good agreement with the deficient adsorption of PAM on silica compared to PEO, as reported by Hackley et al.[56] and the absence of interaction of PAM gels with aerosil particle surfaces.[57] This also explains why PAM-*b*-PAA was not incorporated in large amounts into the mesoPIC hybrid materials, as previously described. In agreement with these results and the XPS data showing the presence of PAM-*b*-PAA on the external surface of small mesoPIC particles, it can be stated that while (PA)PEO-*b*-PAA / OC serves to control the internal silica - pore interface, PAM-*b*-PAA / OC serves to control the external surface of the material dispersed in water and to reduce particle sizes. Scheme 1 summarizes this dual control of particles porosity and morphology.

Scheme 1. Route for the control of internal porous structure and external surface of mesoporous silica particles using mixed polyion complex micelle.

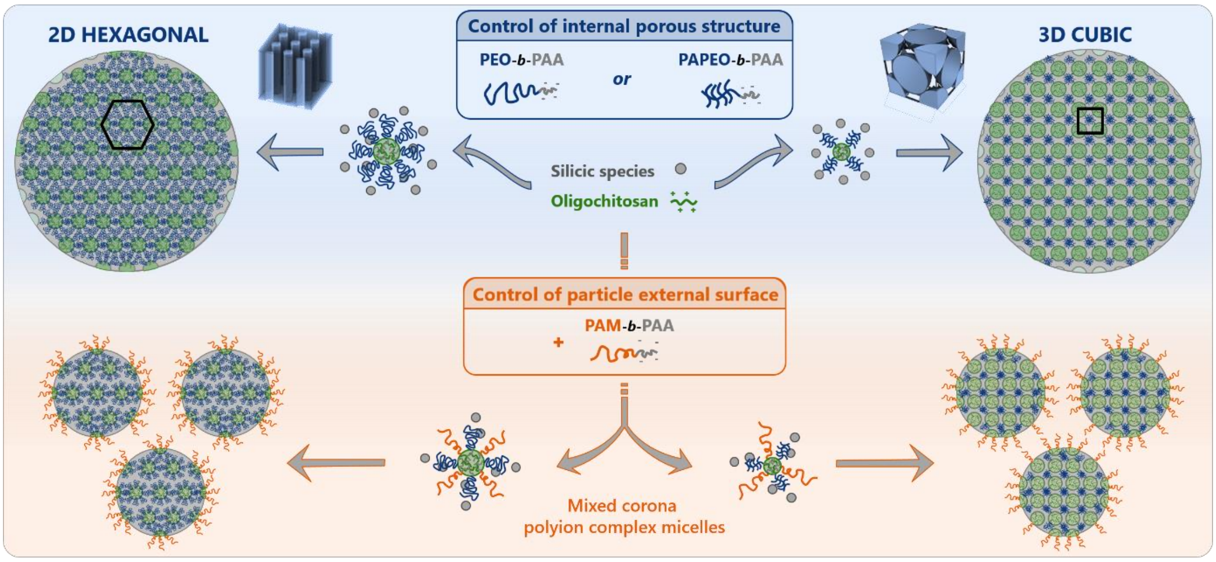

Despite their seemingly distinct roles, PAM-*b*-PAA and PEO-*b*-PAA must first assemble with OC into a mixed corona - PIC assembly for further producing particles of reduced size.

In fact, when PIC micelles with a mixed PAM/PEO corona were promoted by mixing PAM-*b*-PAA and PEO-*b*-PAA together with OC *before* the addition of silicic species, even smaller particles were produced with sizes as small as of 208 nm. On the contrary, when two micellar solutions of PEO-*b*-PAA/OC and PAM-*b*-PAA/OC/silicic species were prepared separately before mixing, larger particles of 945 nm were obtained (see experimental details in section S5 of SI). Furthermore, the presence of the PAA block in PAM-*b*-PAA plays a crucial role in the growing organic/inorganic assembly to control the particle size. Indeed, the addition of a PAM homopolymer (10 000 g/mol) instead of PAM-*b*-PAA copolymer has no effect on particle size or morphology, suggesting the likely anchoring of PAM-*b*-PAA at the particle/water interface via a PAA block complexing OC.

Scheme 2 describes our proposed mechanism for mesoPIC material growth inhibition and particle size reduction. Considering the lack of affinity between silicic species and PAM blocks, we assume that silica species preferentially interact with PEO in the mixed (PA)PEO/PAM corona of the primary PIC assembly. Thus, the more PAM-b-PAA is present in the mixed corona, the weaker the interaction between the micelle corona and silicic species. This would explain why silica walls become thicker as the content of substituted PAM-*b*-PAA increases. The subsequent silica condensation step would then promote (1) silica-PEO condensed domains formed by hydrogen bonding between PEO chains and silicic oligomers and (2) migration and segregation of PAM-*b*-PAA polymers towards the external surface of the forming particles, where they remain anchored through electrostatic complexation with OC to the PIC core at the interface with water. This induces a very homogeneous texture on the particle surface as shown by SEM images that reveal perfectly round, separated and organized organic cores (Fig. 5b) compared to the heterogeneous texture of the particle outer surface obtained in the absence of PAM-*b*-PAA (Fig. 5a). A very important feature of the present PAM-*b*-PAA-based strategy is that it maintains the pore size and topology up to the particle surface. Thus, the PAM blocks act as capping agents, inhibiting the condensation and growth of the material that occur through (PA)PEO/silica interactions. PAM blocks would prevent additional silica species from reaching the (PA)PEO blocks, limiting further growth of the hybrid mesostructure. Furthermore, we propose that the mechanism for growth inhibition proceeds by steric stabilization, thus preventing particle aggregation. This is suggested by the electrokinetics measurements performed on the hybrid materials at pH = 4.8, which reveal an almost neutral zeta potential value for **HEX-40** hybrid colloidal particles (-3.4 ± 0.3 mV) whereas the **HEX-0** material synthesized in the absence of PAM-*b*-PAA shows a significantly negative value (-11.7 ± 0.2 mV) due to the silanolate species. It is then assumed that the presence of PAM chains surrounding the dispersed particles shields the silanolate electrical charges in the double layer, as previously observed by Lee and Somasundaran.[58] As a consequence, this method allows to obtain particles with both low zeta potential (in absolute) and low aggregation (d_{DLS}/d_{TEM} close to 1), factors which can be correlated to a lower cytotoxicity and inflammatory potency.[59]

Scheme 2. Suggested mechanism for reducing the size and controlling the external surface of mesoPIC particles (cross-section representation, not to scale) based on the use of mixed corona polyion complex micelles as structure-directing agents.

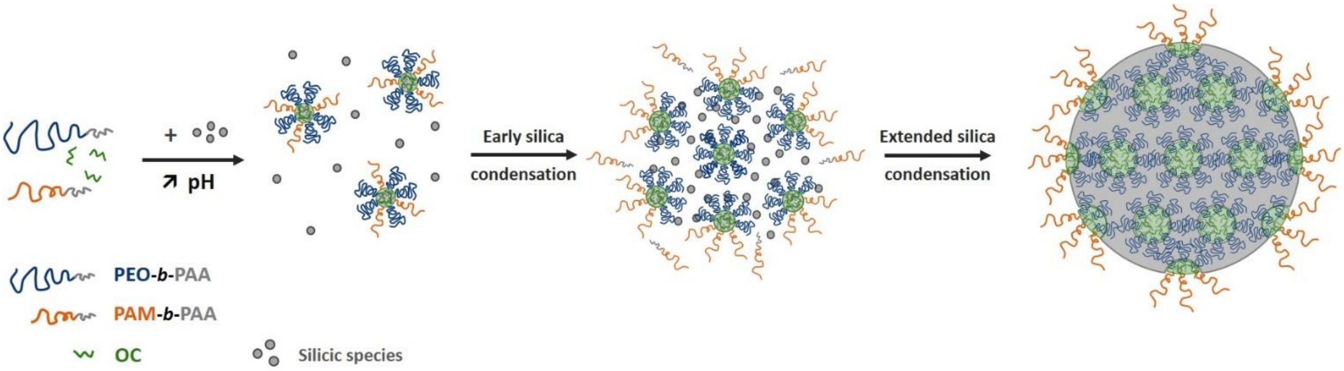

When pH is increased, silica precursors (grey circles) interact with PEO chains (blue) and condense, causing PAM-*b*-PAA segregation on the outer surface of the particles. PAM chains (orange) stay anchored at water/particle interface through complexation with the coacervate AA/OC core, inhibiting growth and preventing aggregation.

In summary, the formation of PIC micelles with mixed corona composed of both PAM and (PA)PEO blocks is a key parameter to govern the stabilization of hybrid particles by PAM through steric control. By decreasing the amount of PAM-*b*-PAA on the particle surface, steric stabilization is reduced, resulting in larger particles. This approach allows reducing particle sizes in the range 220 to 350 nm for **HEX** materials and in the range 350 to 550 nm for **CUB**, by varying the concentration of PAM-*b*-PAA stabilizing agent. A concentration effect to control the size of mesoporous silica nanoparticles templated by conventional cationic surfactants under basic conditions has also been reported using Pluronic triblock copolymers such as P123[60] and F127[23]. The reason why **CUB** particles are larger than **HEX** particles for a similar mass fraction of PAM-*b*-PAA replacing PAPEO-*b*-PAA or PEO-*b*-PAA, respectively, stems from the different architecture of the poly(ethylene oxide) based neutral block, which is known to strongly affect the properties of the neutral block such as size, shape, intrinsic viscosity and miscibility.[61] Here, the lower amount of PAM-*b*-PAA on the surface of **CUB** particles (Section S4) compared to the **HEX** particles suggests a lower miscibility of PAPEO with PAM compared to PEO with PAM. Several factors may explain this lower solubility: 1) a more compact comb-like structure of PAPEO providing C-O-C groups in an unfavorable position for directional bonding with -CONH$_2$ groups in PAM, 2) a poor chain entanglement of linear and brush polymers as observed for PS,[62] 3) a noticeable chain-end effect of PEO compared to the linear polymer of the same molecular weight,[63,64] 4) a higher local concentration of poly(ethylene oxide) in PAPEO unfavoring its mixing with PAM.[53]

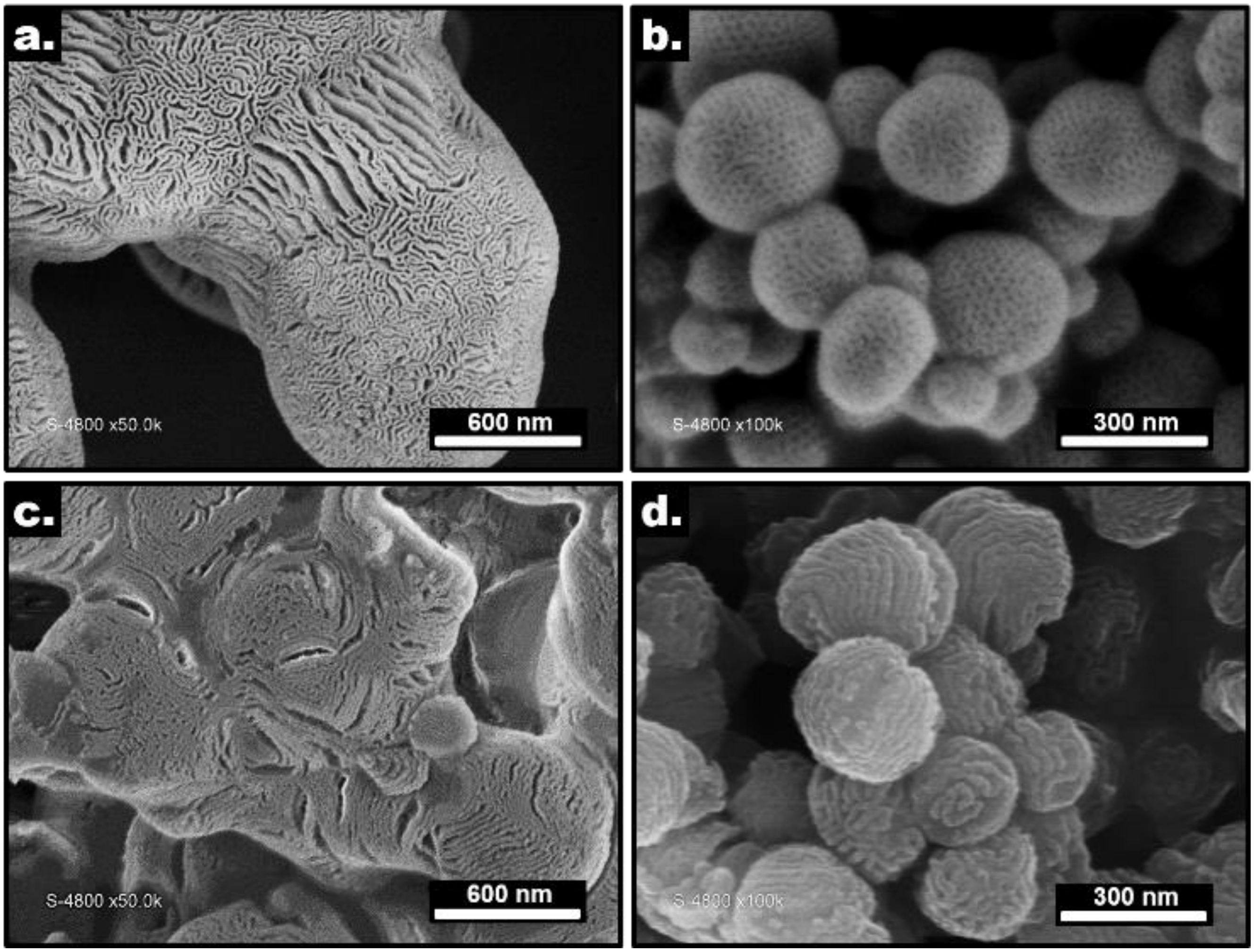

Figure 5. SEM images presenting the surface of hybrid particles of hexagonal structure a) HEX-0, b) HEX-60 and lamellar structure c) LAM-0, d) LAM-40.

Thus, we postulate that the amount of PAM-*b*-PAA stabilizing the external surface of the particle depends only on the mixing of PAM with PAPEO or PEO, regardless of the type of mesostructure. To support this hypothesis, we prepared an additional 2D hexagonal mesostructure from a comb-type PAPEO-*b*-PAA polymer to compare with the reference material of same mesostructure obtained using linear PEO-*b*-PAA. The formation of **HEX** materials using PAPEO-*b*-PAA was successfully achieved by appropriately modifying the initial synthesis conditions (Section S7 of SI) using our expertise in controlling the structure of mesoporous materials by using PIC as structure-directing agent.[30,31] Replacing 40 wt. % PAPEO-*b*-PAA with PAM-*b*-PAA (Section S7) leads to particles with an ordered 2D hexagonal structure exhibiting a larger size (510 nm) compared to that (310 nm) obtained with linear PEO-*b*-PAA. This clearly highlights the role of the PEO-based block configuration in the ability to mix with PAM, and then in the growth control operated by the PAM block.

Interestingly, particle growth control can be tuned by varying the block lengths of the PAM-*b*-PAA copolymer; for example, average **HEX** structure particle sizes of 473 nm instead of 302 nm are obtained when a polymer of half the block length, PAM_{70}-*b*-PAA_{20} (40%), is used instead of PAM_{140}-*b*-PAA_{40} (see Section S7 of SI). This is due to the less effective steric barrier of shorter PAM blocks, as observed in steric stabilization of particles by solvophilic polymers.[65] More importantly, the control of particle growth detailed here for 2D hexagonal and 3D cubic structures was successfully extended to the lamellar mesostructure (**LAM**). We attest that increasing the volume of the electrostatic complex core relative to that of the PEO/inorganic corona enables the formation of highly dispersed lamellar mesoPIC particles. The **LAM** material was thus obtained by using the same PEO-*b*-PAA copolymer in association with a longer oligochitosan and by performing the material condensation step at pH 5.5 (section S8). In the absence of PAM-*b*-PAA, the particle morphology was poorly defined (**LAM**-0, Fig. 5c), whereas by substituting 40% of the PEO-*b*-PAA with PAM-*b*-PAA, small and well dispersed spherical particles with a reduced size of 350 nm were formed (**LAM**-40, Fig. 5d and full characterization in Section S8).

Conclusion

A new route was developed for the synthesis of small well-dispersed mesoporous silica particles with controlled internal pore structure and external particle surface under near-neutral pH conditions at room temperature. The small particles have large mesopores (6 to 10 nm) with tunable long-range ordered topologies: 2D cylindrical hexagonal, 3D cage-like and lamellar structures. The particles are well-dispersed, have a homogeneous morphology and a size reduced to about 200 nm. Their synthesis relies on the use of polyion complex (PIC) micelles consisting of a dual system of PAM-*b*-PAA and PEO-*b*-PAA or PAPEO-*b*-PAA double-hydrophilic block copolymers capable of complexing oligochitosan (OC). The mixed PAM/PEO-based PIC micelles are involved in control of both internal porous structure and external surface of the particles: while the PEO chains interact with silica and drive the formation of the inner silica-pore interface, the PAM chains that have no affinity for silica drive the formation of the outer particle-water interface. In other words, PIC assemblies of PAM and PEO-based DHBC polymers appear as a unique surface control system capable of modulating the inner and the outer surface of the ordered mesoporous particles. The PAM-*b*-PAA polymers, which are anchored by electrostatic complexation with OC through the micellar coacervate core, cap silica particles and limit particle growth, ensuring their colloidal stabilization and preventing their aggregation. The average size of the particles was controlled down to 220 nm for the hexagonal mesostructure and 350 nm for the cubic one, by varying the amount and length of PAM-*b*-PAA. The method was finally extended to the synthesis of small-sized particles with a lamellar mesostructure. A very interesting feature is that PAM-based DHBC anchor to the surface by complexation of the coacervate core and stabilize the pore topology to the outer surface of the particle; thus, they provide highly homogeneous, ordered and open porosity on the outer surface of the particle. The eco-friendly, robust and versatile approach presented here paves the way for large-scale production of small ordered mesoporous particles with user-defined properties.

Corresponding Author

* E-mail: nathalie.marcotte@enscm.fr * Email: corine.gerardin@enscm.fr

Author Contributions

The manuscript was written through contributions of all authors. All authors have given approval to the final version of the manuscript.

Experimental Methods

Chemicals

Oligochitosan (OC) with a molecular mass of 2500 g/mol and a deacetylation degree of 97% (calculated from ^{1}H NMR) was purchased from Creative PegWorks®. TEOS and the following chemicals used in the synthesis of the double hydrophilic block copolymers (DHBC): poly(ethylene glycol) methyl ether acrylate (Mn = 480 g/mol, 8.5 EO units on average), 4,4′-azobis(4-cyanopentanoic acid) (98%) and 2,2’-azobis(isobutyramidine) dihydrochloride (97%) were purchased from Sigma Aldrich and used as received. Acrylamide from SNF (50% in water stabilized with 100 ppm MEHQ) was used as received. Acrylic acid from Sigma Aldrich was distilled under vacuum at room temperature prior to use. PEO with M_n = 10 000 g.mol^{-1} and $\overline{D}$ = 1.04 was purchased from Fluka.

DHBC synthesis

Three double-hydrophilic block copolymers of same molecular weights were synthesized. PEO_{227}-*b*-PAA_{40}, $PAPEO_{20}$-*b*-PAA_{40} and PAM_{140}-*b*-PAA_{40} were synthesized by aqueous RAFT or MADIX polymerization following the procedure published by Phimphachanh et al.[66] The degrees of polymerization of the blocks were determined from ^{1}H NMR and SEC analyses. For all DHBC, the molecular weight of the neutral block (PEO, PAPEO or PAM) is 10000 g.mol^{-1} and the molecular weight of the PAA block is 2880 g.mol^{-1}. DHBC characterizations by ^{1}H NMR and size exclusion chromatography are given in Supporting Information S9.

Preparation of mesoPIC materials

Mesoporous silica materials were prepared by the following one-pot synthesis approaches.

Synthesis of mesoporous materials structured in a 2D hexagonal arrangement

The concentrations of OC and TEOS were fixed with respect to the number of acrylic acid (AA) and ethylene oxide (EO) units of the PEO_{227}-*b*-PAA_{40} DHBC. Equimolar ratios were set between amines and carboxylic groups (N/AA = 1), and for silicon and EO (Si/EO = 1). The final concentration of the reaction medium was set at 2.0 wt% of the DHBC.

Typically, 100 mg of PEO-*b*-PAA were dissolved in a mixture containing 4.5 g of deionized water and 73 mg of OC. The pH of the solution was then adjusted to 2 using H_2SO_4 (1 M), and then 383 mg of TEOS were added. After the solution was stirred at 30°C for 1h, the pH was increased to 4.5 with an aqueous NaOH solution (2 M). The mixture was left under gentle stirring for 5 hours at 30°C. The precipitate formed was then recovered by centrifugation, slightly rinsed with a few droplets of deionized water and air-dried at 80°C for 16 hours. When necessary for characterization purposes, the hybrid materials were calcined in air at 550°C for 8 hours.

Synthesis of mesoporous materials structured in a 3D cubic arrangement

The procedure was similar to that described for the synthesis of the hexagonally structured particles except that $PAPEO_{20}$-*b*-PAA_{40} was used as the DHBC instead of PEO_{227}-*b*-PAA_{40}. The N/AA and EO/Si molar ratios and the concentration of the synthesis medium remained unchanged.

Synthesis of particles of reduced size

For the synthesis of small particles, the procedure was similar to the previous one except that a varying fraction of the PEO_{227}-*b*-PAA_{40} or $PAPEO_{20}$-*b*-PAA_{40} DHBC was substituted by PAM_{140}-*b*-PAA_{40} in the synthesis mixture. The total concentration of DHBC, the N/AA and EO/Si ratios were unchanged. The samples were denoted HEX-X or CUB-X with X corresponding to the percentage of PAM_{140}-*b*-PAA_{40} introduced by substitution.

Characterization methods

Structural characterization

The structure, texture and morphology of the materials were analyzed by TEM, SAXS and nitrogen sorption experiments on samples calcined under air at 550°C for 8h. SEM and DLS analyses were performed on the hybrid materials.

TEM images were acquired using a JEOL 1200 EX II operating at 120 kV. Images were processed using ImageJ software. **SEM** images were acquired using a Hitachi S4800 FEG-HR operating at 12 kV. **SAXS** experiments were done using the homemade instrument described in ref [30] with a copper X-ray tube (λ=1.54 A). **Nitrogen sorption** experiments were performed using a Micromeritics Tristar 3000 after degazing the samples for one night at 250°C under vacuum. Specific areas were calculated using BET equation, volumes of micro- and mesopores were determined using the alpha-S method, and pore size distributions were estimated from the adsorption branch by NDLFT method using Broekhoff et Boer equations.[42] **DLS** measurements of the dispersed particles were performed on a Malvern Autosizer 4800 spectrogoniometer. The dispersions were prepared by sonicating the hybrid particles at 250 ppm in deionized water for 5 minutes. They were analyzed after one hour of rest, without prior filtration.

Calculation of the mean wall thickness h and coherence length L

The coherence lengths ***L*** were calculated from SAXS diffractograms using the following Debye-Scherrer equation:

$$L = \frac{k \times \lambda}{\beta \times \cos\theta}$$

in which k is a corrective factor (here $k = 0.9$), λ the wavelength of the X-ray beam, β the full width at half maximum of the first peak (in radian), and θ stands for the angle of diffraction of the first peak (i.e. q0 in radian). The value of β was corrected from the instrumental resolution of the device such as:

$$\beta^2 = \beta_{exp}^2 - \beta_i^2$$

With β_{exp} the FWHM of the Gaussian fit of the first peak and β_i the instrumental resolution (0.00609 radian here).

The calculation of the mean silica wall thickness $\boldsymbol{h_{mean}}$ was based on geometrical considerations and thus depends on the porous structure of particles. For materials with a hexagonal P6mm structure, the following equation was used:

$$h_{mean} = d_0 \times \frac{2}{\sqrt{3}} - d_{pore}$$

For materials with a cubic structure, the equation reported by Ravikovitch and Neimark was used: [67]

$$h_{mean} = \frac{d_0}{3} \times \left(\frac{6\,\varepsilon_{meso}}{4\,\pi}\right)^{1/3} \times \frac{(1-\varepsilon_{meso})}{\varepsilon_{meso}}$$

In these equations, d_0 stands for the lattice parameter determined by SAXS, d_{pore} is the mean diameter of mesopores determined by N_2 sorption analysis and ε_{meso} the volume fraction of mesopores calculated from the mesoporous volume.[67]

Chemical characterization

Bulk analysis

The chemical composition of the hybrid materials was determined using a combination of data from elemental analysis and thermogravimetric analysis (TGA). TGA was performed using a PerkinElmer STA 6000 apparatus from 30°C to 900°C at a rate of 10°C/min under air flow. The silica content wt. $\%SiO_2$ was considered equal to the residual mass obtained at 900°C. Elemental analysis was performed on a Elementar Vario Micro Cube apparatus to determine the carbon wt. C% and nitrogen wt. N% contents in the hybrid materials. The amount of DHBC (wt. DHBC%) and OC (wt. OC%) in the hybrid mesoPIC materials was then calculated from the following equations:

$$\text{wt. N\%} = \text{wt. OC\%} \times \text{wt. N}_{\text{OC}}\%$$

$$\text{wt. C\%} = \left(\text{wt. OC\%} \times \text{wt. C}_{\text{OC}}\%\right) + \left(\text{wt. DHBC\%} \times \text{wt. C}_{\text{DHBC}}\%\right)$$

It should be noted that the presence of N atoms in PAM-*b*-PAA precludes the determination of DHBC wt.% and OC wt. % when the material is synthesized in the presence of PAM-*b*-PAA.

Spectroscopic measurements were also done by infra-red attenuated total reflectance (IR-ATR) and solid-state Cross-Polarization at Magic Angle Spinning Nuclear Magnetic Resonance (CP-MAS NMR). The **IR-ATR** measurements were performed using a Bruker Vector 22 equipment (λ=633 nm). **NMR** analyses were performed using a Varian VNMRS 400 MHz spectrometer at 293K with a spinning rate of 2 kHz. Adamantane and glycine were used as references for ^{13}C NMR and ^{15}N chemical shifts, respectively.

Surface analysis

Characterizations of the outer surface of hybrid particles were performed by X-ray Photoelectron Spectroscopy (XPS) and Zeta Potential analysis. **XPS** analyses were performed on a Thermo Electron ESCALAB 250 with an Al Kα anode X-ray monochromatic source of 1486.6 eV. The spectra refer to the C 1s peak (284.8 eV) of carbon. Peak deconvolutions were performed with the Origin software. The positions, band widths and area ratios of the NH_2 to NH_3^+ bands of oligochitosan were determined on the commercial crude sample and fixed to those values for fitting of the mesoPIC materials spectra. The position and width of the NHCO band of PAM-*b*-PAA in the HEX-60 and CUB-60 materials were then adjusted to obtain the best fit. Measurements of zeta potentials were done using a Malvern Zetasizer NanoZS instrument on materials dispersed at a concentration of 250 ppm in a buffer solution of acetic acid/sodium acetate (C_{tot}=0.1 M) at pH=4.8. Each measurement was repeated 3 times and the final mean value was reported. Debye length $\boldsymbol{\kappa}^{-1}$ was calculated with the following simplified equation for electrolyte aqueous solution at 298K:

$$\boldsymbol{\kappa}^{-1} = \frac{0.304}{\sqrt{I}}$$

Acknowledgements

The authors thank Philippe Gaveau and Emmanuel Fernandez for NMR experiments. This work was financially supported by the French National Research Agency (ANR grant n°15-CE07-0005).

Supporting Information

Supporting Information available:

- Textural properties and chemical composition of mesoPIC materials
- Supplementary solid state NMR, ATR-FTIR, XPS spectra of hybrid mesoPIC materials
- Influence of the synthesis process on the size of the particles
- Synthesis of HEX structure using PAPEO-*b*-PAA
- Influence of the PAM-*b*-PAA chain length on the size of the particles
- Formation of lamellar mesoPIC particles
- Characterization of DHBC polymers

References

[1] L.T. Gibson, Mesosilica materials and organic pollutant adsorption: Part A removal from air, Chem. Soc. Rev. 43 (2014) 5163–5172. https://doi.org/10.1039/C3CS60096C.

[2] A. Corma, From Microporous to Mesoporous Molecular Sieve Materials and Their Use in Catalysis, Chem. Rev. 97 (1997) 2373–2420. https://doi.org/10.1021/cr960406n.

[3] J. Wei, Z. Sun, W. Luo, Y. Li, A.A. Elzatahry, A.M. Al-Enizi, Y. Deng, D. Zhao, New insight into the synthesis of large-pore ordered mesoporous materials, J. Am. Chem. Soc. 139 (2017) 1706–1713. https://doi.org/10.1021/jacs.6b11411.

[4] M. Abbasi, S.H. Ghoran, M.H. Niakan, K. Jamali, Z. Moeini, A. Jangjou, P. Izadpanah, A.M. Amani, Mesoporous silica nanoparticle: Heralding a brighter future in cancer nanomedicine, Microporous Mesoporous Mater. 319 (2021) 110967. https://doi.org/10.1016/j.micromeso.2021.110967.

[5] E. Yamamoto, K. Kuroda, Colloidal mesoporous silica nanoparticles, Bull. Chem. Soc. Jpn. 89 (2016) 501–539. https://doi.org/10.1246/bcsj.20150420.

[6] I.I. Slowing, J.L. Vivero-Escoto, B.G. Trewyn, V.S.-Y. Lin, Mesoporous silica nanoparticles: structural design and applications, J. Mater. Chem. 20 (2010) 7924. https://doi.org/10.1039/c0jm00554a.

[7] K. Möller, T. Bein, Talented mesoporous silica nanoparticles, Chem. Mater. 29 (2017) 371–388. https://doi.org/10.1021/acs.chemmater.6b03629.

[8] R. Narayan, U. Nayak, A. Raichur, S. Garg, R. Narayan, U.Y. Nayak, A.M. Raichur, S. Garg, Mesoporous Silica Nanoparticles: A Comprehensive Review on Synthesis and Recent Advances, Pharmaceutics. 10 (2018) 118. https://doi.org/10.3390/pharmaceutics10030118.

[9] T. Zhao, L. Chen, R. Lin, P. Zhang, K. Lan, W. Zhang, X. Li, D. Zhao, Interfacial Assembly Directed Unique Mesoporous Architectures: From Symmetric to Asymmetric, Accounts Mater. Res. 1 (2020) 100–114. https://doi.org/10.1021/accountsmr.0c00028.

[10] C.E. Fowler, D. Khushalani, B. Lebeau, S. Mann, Nanoscale materials with mesostructured interiors, Adv. Mater. 13 (2001) 649–652. https://doi.org/10.1002/1521-4095(200105)13:9<649::AID-ADMA649>3.0.CO;2-G.

[11] R.I. Nooney, D. Thirunavukkarasu, C. Yimei, R. Josephs, A.E. Ostafin, Synthesis of nanoscale mesoporous silica spheres with controlled particle size, Chem. Mater. 14 (2002)

4721–4728. https://doi.org/10.1021/cm0204371.

[12] Q. Cai, Z.-S. Luo, W.-Q. Pang, Y.-W. Fan, X.-H. Chen, F.-Z. Cui, Dilute Solution Routes to Various Controllable Morphologies of MCM-41 Silica with a Basic Medium, Chem. Mater. 13 (2001) 258–263. https://doi.org/10.1021/cm990661z.

[13] F. Lu, S.-H. Wu, Y. Hung, C.-Y. Mou, Size Effect on Cell Uptake in Well-Suspended, Uniform Mesoporous Silica Nanoparticles, Small. 5 (2009) 1408–1413. https://doi.org/10.1002/smll.200900005.

[14] I.I. Slowing, B.G. Trewyn, V.S.Y. Lin, Mesoporous silica nanoparticles for intracellular delivery of membrane-impermeable proteins, J. Am. Chem. Soc. 129 (2007) 8845–8849. https://doi.org/10.1021/ja0719780.

[15] T. Ribeiro, A.S. Rodrigues, S. Calderon, A. Fidalgo, J.L.M. Gonçalves, V. André, M. Teresa Duarte, P.J. Ferreira, J.P.S. Farinha, C. Baleizão, Silica nanocarriers with user-defined precise diameters by controlled template self-assembly, J. Colloid Interface Sci. 561 (2020) 609–619. https://doi.org/10.1016/j.jcis.2019.11.036.

[16] S. Sadasivan, D. Khushalani, S. Mann, Synthesis and shape modification of organo-functionalised silica nanoparticles with ordered mesostructured interiors, J. Mater. Chem. 13 (2003) 1023–1029. https://doi.org/10.1039/b300851g.

[17] K. Möller, J. Kobler, T. Bein, Colloidal suspensions of nanometer-sized mesoporous silica, Adv. Funct. Mater. 17 (2007) 605–612. https://doi.org/10.1002/adfm.200600578.

[18] T. Yokoi, J. Wakabayashi, Y. Otsuka, W. Fan, M. Iwama, R. Watanabe, K. Aramaki, A. Shimojima, T. Tatsumi, T. Okubo, Mechanism of formation of uniform-sized silica nanospheres catalyzed by basic amino acids, Chem. Mater. 21 (2009) 3719–3729. https://doi.org/10.1021/cm900993b.

[19] K. Suzuki, K. Ikari, H. Imai, Synthesis of Silica Nanoparticles Having a Well-Ordered Mesostructure Using a Double Surfactant System, J. Am. Chem. Soc. 126 (2004) 462–463. https://doi.org/10.1021/ja038250d.

[20] Y. Han, J.Y. Ying, Generalized fluorocarbon-surfactant-mediated synthesis of nanoparticles with various mesoporous structures, Angew. Chemie - Int. Ed. 44 (2004) 288–292. https://doi.org/10.1002/anie.200460892.

[21] F. Gao, P. Botella, A. Corma, J. Blesa, L. Dong, Monodispersed Mesoporous Silica Nanoparticles with Very Large Pores for Enhanced Adsorption and Release of DNA, J.

Phys. Chem. B. 113 (2009) 1796–1804. https://doi.org/10.1021/jp807956r.

[22] Y. Lu, H. Fan, A. Stump, T.L. Ward, T. Rieker, C.J. Brinker, Aerosol-assisted self-assembly of mesostructured spherical nanoparticles, Nature. 398 (1999) 223–226. https://doi.org/10.1038/18410.

[23] T.-W. Kim, P.-W. Chung, V.S.-Y. Lin, Facile Synthesis of Monodisperse Spherical MCM-48 Mesoporous Silica Nanoparticles with Controlled Particle Size, Chem. Mater. 22 (2010) 5093–5104. https://doi.org/10.1021/cm1017344.

[24] R. Sun, P. Qiao, Z. Wang, W. Wang, Monodispersed large-mesopore mesoporous silica nanoparticles enabled by sulfuric acid assisted hydrothermal process, Microporous Mesoporous Mater. 317 (2021) 111023. https://doi.org/10.1016/j.micromeso.2021.111023.

[25] Z. Wang, R. Sun, P. Wang, W. Wang, Unit-cell wide SBA-15 type mesoporous silica nanoparticles, Microporous Mesoporous Mater. 328 (2021) 111491. https://doi.org/10.1016/j.micromeso.2021.111491.

[26] Z.A. Qiao, L. Zhang, M. Guo, Y. Liu, Q. Huo, Synthesis of mesoporous silica nanoparticles via controlled hydrolysis and condensation of silicon alkoxide, Chem. Mater. 21 (2009) 3823–3829. https://doi.org/10.1021/cm901335k.

[27] K. Zhang, L.L. Xu, J.G. Jiang, N. Calin, K.F. Lam, S.J. Zhang, H.H. Wu, G.D. Wu, B. Albela, L. Bonneviot, P. Wu, Facile large-scale synthesis of monodisperse mesoporous silica nanospheres with tunable pore structure, J. Am. Chem. Soc. 135 (2013) 2427–2430. https://doi.org/10.1021/ja3116873.

[28] N. Baccile, J. Reboul, B. Blanc, B. Coq, P. Lacroix-Desmazes, M. In, C. Gerardin, Ecodesign of ordered mesoporous materials obtained with switchable micellar assemblies, Angew. Chemie. 47 (2008) 8433–8437. https://doi.org/10.1002/anie.200802431.

[29] J. Warnant, N. Marcotte, J. Reboul, G. Layrac, A. Aqil, C. Jerôme, D.A. Lerner, C. Gérardin, Physicochemical properties of pH-controlled polyion complex (PIC) micelles of poly(acrylic acid)-based double hydrophilic block copolymers and various polyamines, Anal. Bioanal. Chem. 403 (2012) 1395–1404. https://doi.org/10.1007/s00216-012-5947-1.

[30] E. Molina, M. Mathonnat, J. Richard, P. Lacroix-Desmazes, M. In, P. Dieudonné, T. Cacciaguerra, C. Gérardin, N. Marcotte, pH-mediated control over the mesostructure of ordered mesoporous materials templated by polyion complex micelles, Beilstein J. Nanotechnol. 10 (2019) 144–156. https://doi.org/10.3762/bjnano.10.14.

[31] D. Houssein, J. Warnant, E. Molina, T. Cacciaguerra, C. Gérardin, N. Marcotte, Mesoporous silica templated by polyion complex micelles: A versatile approach for controlling the mesostructure, Microporous Mesoporous Mater. 239 (2017) 244–252. https://doi.org/http://dx.doi.org/10.1016/j.micromeso.2016.10.013.

[32] N. Mebarek, A. Aubert-Pouëssel, C. Gérardin, R. Vicente, J.M. Devoisselle, S. Bégu, Polymeric micelles based on poly(methacrylic acid) block-containing copolymers with different membrane destabilizing properties for cellular drug delivery, Int. J. Pharm. 454 (2013) 611–620. https://doi.org/10.1016/j.ijpharm.2013.06.014.

[33] A. Birault, E. Molina, C. Carcel, J. Bartlett, N. Marcotte, G. Toquer, P. Lacroix-Desmazes, C. Gerardin, M. Wong Chi Man, Synthesis of lamellar mesostructured phenylene-bridged periodic mesoporous organosilicas (PMO) templated by polyion complex (PIC) micelles, J. Sol-Gel Sci. Technol. 89 (2019) 189–195. https://doi.org/10.1007/s10971-018-4667-1.

[34] E. Molina, J. Warnant, M. Mathonnat, M. Bathfield, M. In, D. Laurencin, C. Jérôme, P. Lacroix-Desmazes, N. Marcotte, C. Gérardin, Drug–Polymer Electrostatic Complexes as New Structuring Agents for the Formation of Drug-Loaded Ordered Mesoporous Silica, Langmuir. 31 (2015) 12839–12844. https://doi.org/10.1021/acs.langmuir.5b03221.

[35] A. Birault, E. Molina, G. Toquer, P. Lacroix-Desmazes, N. Marcotte, C. Carcel, M. Katouli, J.R. Bartlett, C. Gérardin, M. Wong Chi Man, Large-Pore Periodic Mesoporous Organosilicas as Advanced Bactericide Platforms, ACS Appl. Bio Mater. 1 (2018) 1787–1792. https://doi.org/10.1021/acsabm.8b00474.

[36] A. Birault, E. Molina, P. Trens, D. Cot, G. Toquer, N. Marcotte, C. Carcel, J.R. Bartlett, C. Gérardin, M. Wong Chi Man, Periodic Mesoporous Organosilicas from Polyion Complex Micelles – Effect of Organic Bridge on Nanostructure, Eur. J. Inorg. Chem. 2019 (2019) 3157–3164. https://doi.org/10.1002/ejic.201900487.

[37] L. Sierra, J.L. Guth, Synthesis of mesoporous silica with tunable pore size from sodium silicate solutions and a polyethylene oxide surfactant, Microporous Mesoporous Mater. 27 (1999) 243–253. https://doi.org/10.1016/S1387-1811(98)00258-3.

[38] L. Sierra, B. Lopez, J.L. Guth, Preparation of mesoporous silica particles with controlled morphology from sodium silicate solutions and a non-ionic surfactant at pH values between 2 and 6, Microporous Mesoporous Mater. 39 (2000) 519–527. https://doi.org/10.1016/S1387-1811(00)00227-4.

[39] C. Gérardin, N. Sanson, F. Bouyer, F. Fajula, J.-L. Putaux, M. Joanicot, T. Chopin, Highly Stable Metal Hydrous Oxide Colloids by Inorganic Polycondensation in Suspension, Angew. Chemie Int. Ed. 42 (2003) 3681–3685. https://doi.org/10.1002/anie.200350917.

[40] G. Layrac, M. Destarac, C. Gérardin, D. Tichit, Highly stable layered double hydroxide colloids: A direct aqueous synthesis route from hybrid polyion complex micelles, Langmuir. 30 (2014) 9663–9671. https://doi.org/10.1021/la502159x.

[41] F. Bouyer, N. Sanson, M. Destarac, C. Gérardin, Hydrophilic block copolymer-directed growth of lanthanum hydroxide nanoparticles, New J. Chem. 30 (2006) 399–408. https://doi.org/10.1039/b516368d.

[42] J.C.P. Broekhoff, J.H. De Boer, Studies on pore systems in catalysts: X. Calculations of pore distributions from the adsorption branch of nitrogen sorption isotherms in the case of open cylindrical pores B. Applications, J. Catal. 9 (1967) 15–27. https://doi.org/https://doi.org/10.1016/0021-9517(67)90175-3.

[43] W. Jia, J. Tian, P. Bai, S. Li, H. Zeng, W. Zhang, Y. Tian, A novel comb-typed poly(oligo(ethylene glycol) methylether acrylate) as an excellent aqueous lubricant, J. Colloid Interface Sci. 539 (2019) 342–350. https://doi.org/10.1016/j.jcis.2018.12.085.

[44] R.E. van Vliet, H.C.J. Hoefsloot, P.D. Iedema, Mesoscopic simulation of polymer–solvent phase separation: linear chain behaviour and branching effects, Polymer (Guildf). 44 (2003) 1757–1763. https://doi.org/10.1016/S0032-3861(03)00023-5.

[45] Z.-C. Yan, D. Vlassopoulos, Chain dimensions and dynamic dilution in branched polymers, Polymer (Guildf). 96 (2016) 35–44. https://doi.org/10.1016/j.polymer.2016.04.058.

[46] J.Y.T. Chong, X. Mulet, A. Postma, D.J. Keddie, L.J. Waddington, B.J. Boyd, C.J. Drummond, Novel RAFT amphiphilic brush copolymer steric stabilisers for cubosomes: Poly(octadecyl acrylate)-block-poly(polyethylene glycol methyl ether acrylate), Soft Matter. 10 (2014) 6666–6676. https://doi.org/10.1039/c4sm01064g.

[47] M.W. Matsen, F.S. Bates, Conformationally asymmetric block copolymers, J. Polym. Sci. Part B Polym. Phys. 35 (1997) 945–952. https://doi.org/10.1002/(SICI)1099-0488(19970430)35:6<945::AID-POLB9>3.0.CO;2-G.

[48] G. Lawrie, I. Keen, B. Drew, A. Chandler-Temple, L. Rintoul, P. Fredericks, L. Grøndahl, Interactions between alginate and chitosan biopolymers characterized using FTIR and XPS, Biomacromolecules. 8 (2007) 2533–2541. https://doi.org/10.1021/bm070014y.

[49] I.F. Amaral, P.L. Granja, M.A. Barbosa, Chemical modification of chitosan by phosphorylation: An XPS, FT-IR and SEM study, J. Biomater. Sci. Polym. Ed. 16 (2005) 1575–1593. https://doi.org/10.1163/156856205774576736.

[50] A. Sundblom, C.L.P. Oliveira, J.S. Pedersen, A.E.C. Palmqvist, On the Formation Mechanism of Pluronic-Templated Mesostructured Silica, J. Phys. Chem. C. 114 (2010) 3483–3492. https://doi.org/10.1021/jp100087z.

[51] D. Zhao, Q. Huo, J. Feng, B.F. Chmelka, G.D. Stucky, Nonionic Triblock and Star Diblock Copolymer and Oligomeric Surfactant Syntheses of Highly Ordered, Hydrothermally Stable, Mesoporous Silica Structures, J. Am. Chem. Soc. 120 (1998) 6024–6036. https://doi.org/10.1021/ja974025i.

[52] J. Warnant, J. Reboul, A. Aqil, T. Cacciaguerra, C. Jerome, C. Gerardin, Nanostructured silica templated by double hydrophilic block copolymers with a comb-like architecture, Powder Technol. 208 (2011) 461–466. https://doi.org/10.1016/j.powtec.2010.08.043.

[53] T. Lü, G. Shan, S. Shang, Intermolecular interaction in aqueous solution of binary blends of poly(acrylamide) and poly(ethylene glycol), J. Appl. Polym. Sci. 118 (2010) 2572–2581. https://doi.org/10.1002/app.32556.

[54] M.M. Abutalib, A. Rajeh, Influence of ZnO/Ag nanoparticles doping on the structural, thermal, optical and electrical properties of PAM/PEO composite, Phys. B Condens. Matter. 578 (2020) 411796. https://doi.org/10.1016/j.physb.2019.411796.

[55] M.E.S.R. Silva, V. Mano, R.R.J. Pacheco, R.F.S. Freitas, Miscibility Behavior of Polyacrylamides Poly(Ethylene Glycol) Blends: Flory Huggins Interaction Parameter Determined by Thermal Analysis, J. Mod. Phys. 04 (2013) 45–51. https://doi.org/10.4236/jmp.2013.47a2007.

[56] V. Hackley, P. Somasundaran, J. Lewis, Polymers in Particulate Systems: Properties and Applications, CRC Press, 2001. https://books.google.fr/books?id=I0VZDwAAQBAJ.

[57] T. V. Terziyan, A.P. Safronov, Y.G. Belous, Interaction of aerosil nanoparticles with networks of polyacrylamide, poly(acrylic acid), and poly(methacrylic acid) hydrogels, Polym. Sci. Ser. A. 57 (2015) 200–208. https://doi.org/10.1134/S0965545X15020169.

[58] L.T. Lee, P. Somasundaran, Adsorption of Polyacrylamide on Oxide Minerals, Langmuir. 5 (1989) 854–860. https://doi.org/10.1021/la00087a047.

[59] D. Breznan, D.D. Das, C. MacKinnon-Roy, S. Bernatchez, A. Sayari, M. Hill, R. Vincent,

P. Kumarathasan, Physicochemical Properties Can Be Key Determinants of Mesoporous Silica Nanoparticle Potency in Vitro, ACS Nano. 12 (2018) 12062–12079. https://doi.org/10.1021/acsnano.8b04910.

[60] K. Ikari, K. Suzuki, H. Imai, Structural control of mesoporous silica nanoparticles in a binary surfactant system, Langmuir. 22 (2006) 802–806. https://doi.org/10.1021/la0525527.

[61] H. Takeshita, T. Shiomi, T. Suzuki, T. Sato, M. Miya, Miscibility in blends of linear and branched poly(ethylene oxide) with methacrylate derivative random copolymers and estimation of segmental c parameters, Polymer (Guildf). 46 (2005) 11463–11469. https://doi.org/10.1016/j.polymer.2005.10.067.

[62] Y. Tsukahara, M. Miyata, K. Senoo, N. Yoshimoto, K. Kyoji, Mesomorphic Phase Formation of Poly(macromonomer)s of Polystyrene Macromonomers, Polym. Adv. Technol. 11 (2000) 210–218.

[63] M. Zhang, A.H.E. Müller, Cylindrical polymer brushes, J. Polym. Sci. Part A Polym. Chem. 43 (2005) 3461–3481. https://doi.org/10.1002/pola.20900.

[64] C. Feng, Y. Li, D. Yang, J. Hu, X. Zhang, X. Huang, Well-defined graft copolymers: From controlled synthesis to multipurpose applications, Chem. Soc. Rev. 40 (2011) 1282–1295. https://doi.org/10.1039/b921358a.

[65] P. Lacroix-Desmazes, A. Guyot, Reactive surfactants in heterophase polymerization Part IV : Dispersion polymerization of styrene and methyl, Colloid Polym Sci. 274 (1996) 1129–1136. https://link.springer.com/article/10.1007/BF00655683.

[66] A. Phimphachanh, J. Chamieh, L. Leclercq, S. Harrisson, M. Destarac, P. Lacroix-Desmazes, C. Gérardin, M. In, H. Cottet, Characterization of Diblock Copolymers by Capillary Electrophoresis: From Electrophoretic Mobility Distribution to Distribution of Composition, Macromolecules. 53 (2020) 334–345. https://doi.org/10.1021/acs.macromol.9b01978.

[67] P.I. Ravikovitch, A. V Neimark, Density functional theory of adsorption in spherical cavities and pore size characterization of templated nanoporous silicas with cubic and three-dimensional hexagonal structures, Langmuir. 18 (2002) 1550–1560. https://doi.org/10.1021/la0107594.

Dual control of external surface and internal pore structure of small ordered mesoporous silica particles directed by mixed polyion complex micelles

Supporting Information

Jason Richard,[a] *Anthony Phimphachanh,* [a,b] *Alix Jamet-Fournier,* [a] *Thomas Cacciaguerra,*[a]

Philippe Dieudonné-George,[b] *Didier Cot,*[c] *Mathias Destarac,*[d] *Patrick Lacroix-Desmazes,*[a]

Martin In,[b] *Nathalie Marcotte** [a] *and Corine Gérardin** [a]

[a] Institut Charles Gerhardt, Univ Montpellier, CNRS, ENSCM, Montpellier, France

[b] Laboratoire Charles Coulomb, Univ Montpellier, CNRS, Montpellier, France

[c] Institut Européen des Membranes, Univ Montpellier, CNRS, ENSCM, Montpellier, France

[d] Pr. M. Destarac, IMRCP, Université Toulouse III, CNRS, Toulouse, France

* E-mail: nathalie.marcotte@enscm.fr, corine.gerardin@enscm.fr

S1. Textural properties and chemical composition of mesoPIC materials

The cage-like cubic (**HEX-X**) and P6mm hexagonal (**CUB-X**) structures obtained by substituting **X** % of the PEO-based copolymer with PAM-*b*-PAA were characterized by SEM before calcination, and by TEM (Fig. S1a), SAXS and nitrogen sorption analysis after calcination. The textural properties of the calcined samples are listed in Table S1a. When the PAM-*b*-PAA% increases, the silica wall thickness linearly increases in both the **HEX** and **CUB** mesoporous materials (Table S1a, Fig. 2e). This thickening of silica walls follows the increase of the cell parameter d0. Meanwhile, the pore diameter decreases for **HEX** materials and remains constant for **CUB** structures (Fig. S1b, Fig. 2f). As a result, these evolutions cause a decrease of the mesoporous volume when the PAM-*b*-PAA% increases.

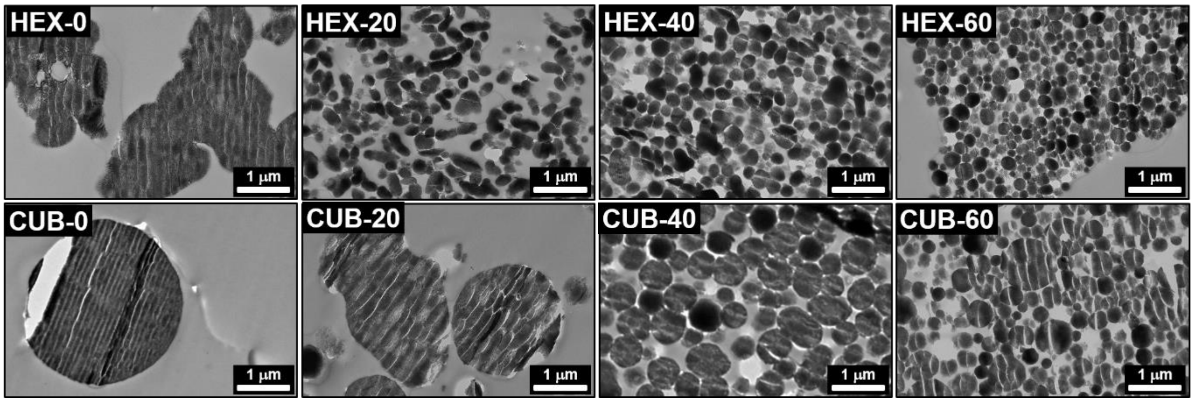

Fig. S1a: TEM images of the microtome-cut calcined mesoPIC particles for the HEX-X (first row), and CUB-X (second row) series obtained with increasing amount of PAM-*b*-PAA.

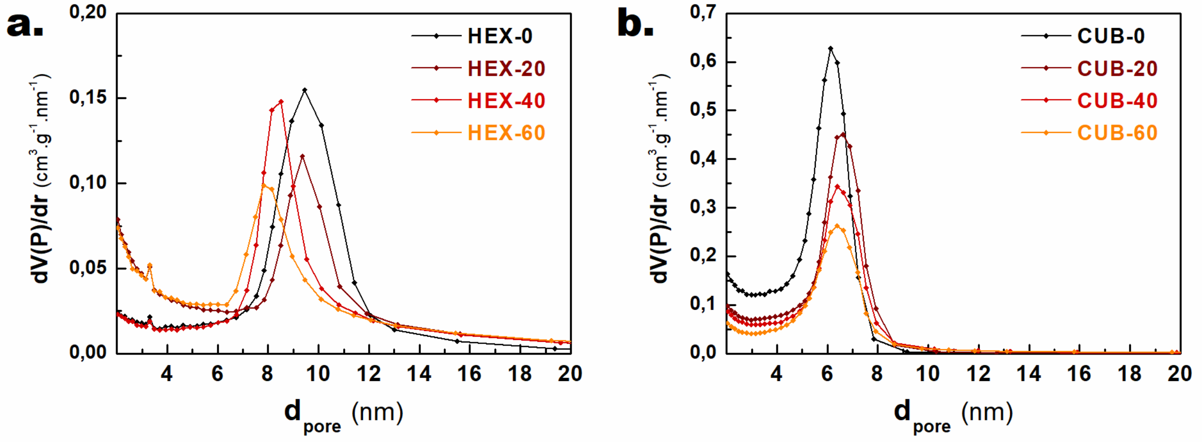

Fig. S1b: pore size distribution of HEX-X (a) and CUB-X (b) calcined mesoPIC materials depending on the amount of PAM-*b*-PAA introduced in the synthesis.

Table S1a: structural and textural properties of calcined mesoPIC materials.

Sample	Φ_{TEM} (nm)	L [a] (nm)	d0 (nm)	V_{micro} (cm^3/g)	V_{meso} [b] (cm^3/g)	V_{inter} [c] (cm^3/g)	d_{pore} (nm)	h_{mean} [d] (nm)	S_{BET} (m^2/g)
HEX-0	> 1000	152	16.5	0.05	0.30	0.03	10.0	9.1	426
HEX-20	309	83	17.5	0.05	0.26	0.09	9.4	10.8	393
HEX-40	302	68	17.2	0.06	0.24	0.12	8.4	11.5	366
HEX-60	228	68	18.2	0.06	0.22	0.15	7.9	13.1	351
CUB-0	> 1000	62	10.3	0.06	0.55	0.01	6.2	2.0	705
CUB-20	> 1000	69	11.0	0.05	0.43	0.01	6.6	2.6	536
CUB-40	542	63	11.3	0.07	0.38	0.03	6.4	3.1	545
CUB-60	354	56	11.4	0.07	0.34	0.07	6.4	3.3	497

[a] coherence length calculated using the Debye-Scherrer equation on the first peak of SAXS diffractograms. [b] V_{meso} measured at p/p°=0.85 after substraction of V_{micro}. [c] V_{inter} measured at p/p°=0.975 after substraction of V_{meso} and V_{micro}. [d] Mean silica walls thickness.

For a given mesostructure, the composition of the hybrid materials remains nearly the same whatever the amount of PAM-*b*-PAA introduced in the synthesis medium.

Table S1b: chemical composition of hybrid mesoPIC materials.

	HEX-0	HEX-20	HEX-40	HEX-60	CUB-0	CUB-20	CUB-40	CUB-60
wt. % SiO_2	49%	50%	50%	50%	43%	42%	44%	44%
wt.% organic	51%	50%	50%	50%	57%	58%	56%	56%

S2. Solid state NMR spectra of hybrid mesoPIC materials

S2.1 ^{13}C CP-MAS NMR

Fig. S2a (left) shows the ^{13}C CP-MAS NMR spectra of **HEX-0** synthesized without PAM-*b*-PAA and of **HEX-50** synthesized with 50% of PAM-*b*-PAA. The attribution of the peaks is done by comparison with the NMR spectra of the crude polymers used to synthesize the mesoPIC hybrid materials, i.e. oligochitosan, PEO-*b*-PAA and PAM-*b*-PAA (Fig. S2a, right). The ^{13}C NMR spectra of **HEX-0** and **HEX-50** are very similar and do not show any obvious fingerprint of PAM-*b*-PAA, which is yet used in high amount in the synthesis of **HEX-50**. Indeed, the characteristic 13C NMR peaks of PAM-*b*-PAA at ~ 42 ppm for the -CH_2- backbone and 182 ppm for –COOH and –$CONH_2$ [1] are present as wide signals both in the **HEX-50** hybrid material and **HEX-0**, which is synthesized without any PAM-*b*-PAA. This impedes the presence of PAM-*b*-PAA in the **HEX-50** hybrid material to be certified, and also suggests its presence in low amount, if any. Thus, the signals at 45 and 182 ppm in **HEX-0** and **HEX-50** more probably arise from carbon sites respectively belonging to the -CH_2- backbone and carboxylic functions of PEO-*b*-PAA,[2] as does the signal of ether functions observed at 74 ppm.[3] Some of the typical signals of oligochitosan at ~60 and 100 ppm clearly reveal the presence of OC in the hybrid materials.

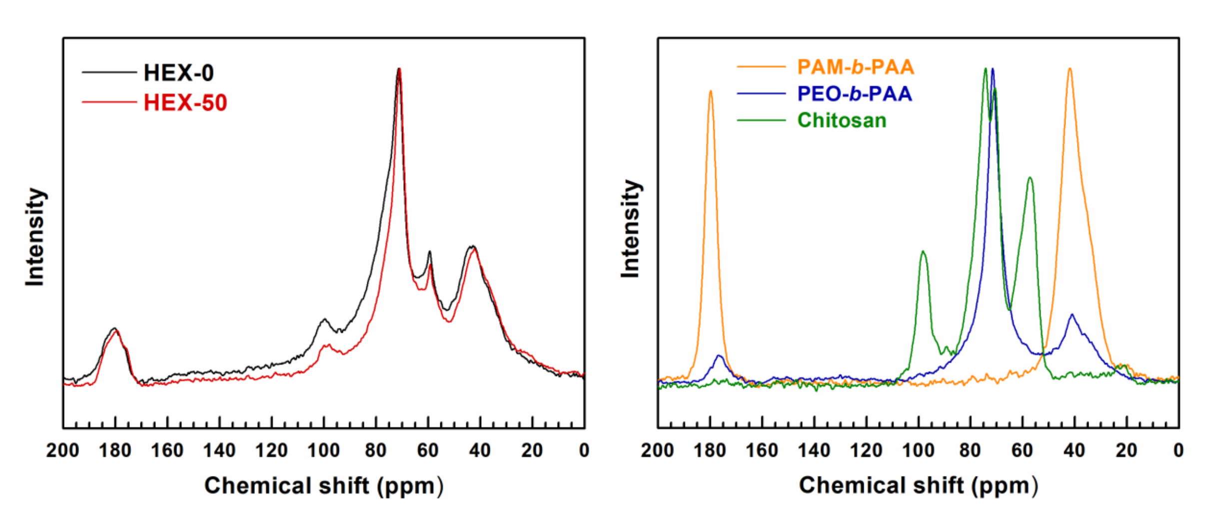

Fig. S2a: ^{13}C CPMAS NMR spectra of (left) hybrid mesoPIC materials prepared without PAM-*b*-PAA (HEX-0) and with 50% of PAM-*b*-PAA (HEX-50) and (right) PAM-*b*-PAA, PEO-*b*-PAA and oligochitosan.

S2.2 ^{15}N CP-MAS NMR

The presence of PAM-*b*-PAA in **CUB-50** was also attempted to be evidenced using ^{15}N CP-MAS NMR (Fig. S2b, left). The spectrum of PAM-*b*-PAA (Fig. S2b, right) exhibits a single signal around 115 ppm assigned to the nitrogen of amide functions of the PAM block. This signal was not observed on the **CUB-50** spectrum (of low signal-to-noise ratio) after an acquisition period of 60h, where only one signal at 30 ppm due to the nitrogen of amine functions of oligochitosan was observed.[4]

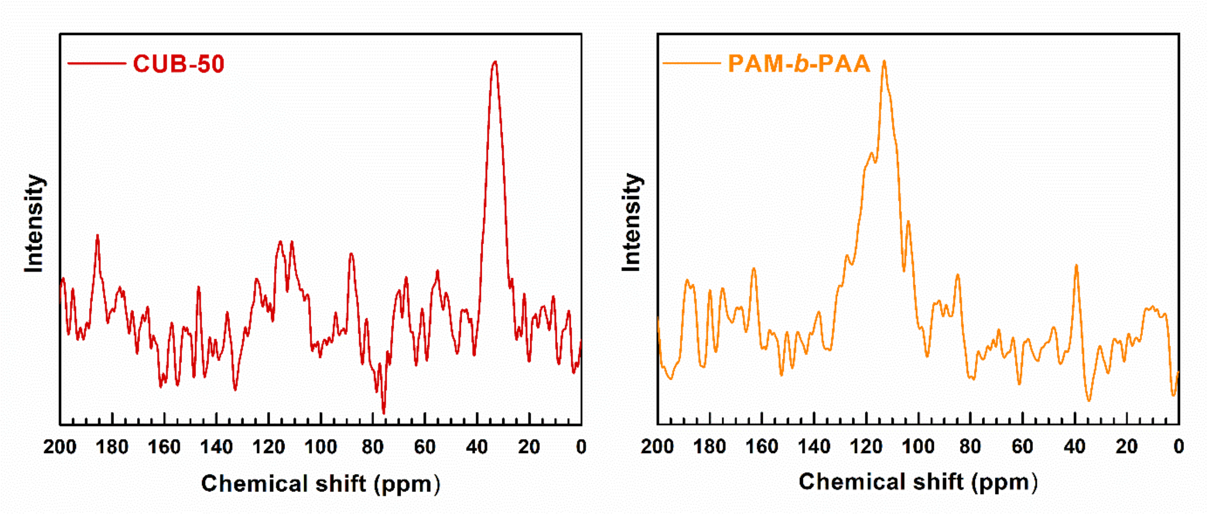

Fig. S2b: ^{15}N CP-MAS NMR spectra of (right) PAM-*b*-PAA and (left) hybrid mesoPIC materials CUB-50 prepared with 50% of PAM-*b*-PAA.

S3. ATR-FTIR spectra of hybrid mesoPIC materials

HEX-0 synthesized without PAM-*b*-PAA and **HEX-60** synthesized with 60% of PAM-*b*-PAA were analyzed by Fourier-transform Infra-red spectroscopy in Attenuated Total Reflectance mode (ATR-FTIR) to look for the presence of PAM-*b*-PAA in the **HEX-60** particles. The spectra were characterized by comparison with the spectrum of the PAM-*b*-PAA DHBC in the range 1800 cm^{-1} - 400 cm^{-1} (Fig. S3).

The PAM-*b*-PAA spectrum is characterized by two intense peaks pointing at 1600 cm^{-1} and 1650 cm^{-1}, respectively assigned to the C=O stretching vibration and N-H deformation vibration of amide functions. These peaks are not observed in the IR spectrum of the **HEX-60** material, which is similar to the spectrum of the **HEX-0** material synthesized without PAM-*b*-PAA. This supports a likely low content of PAM-*b*-PAA within the particles, as concluded from the solid state NMR studies of the previous section.

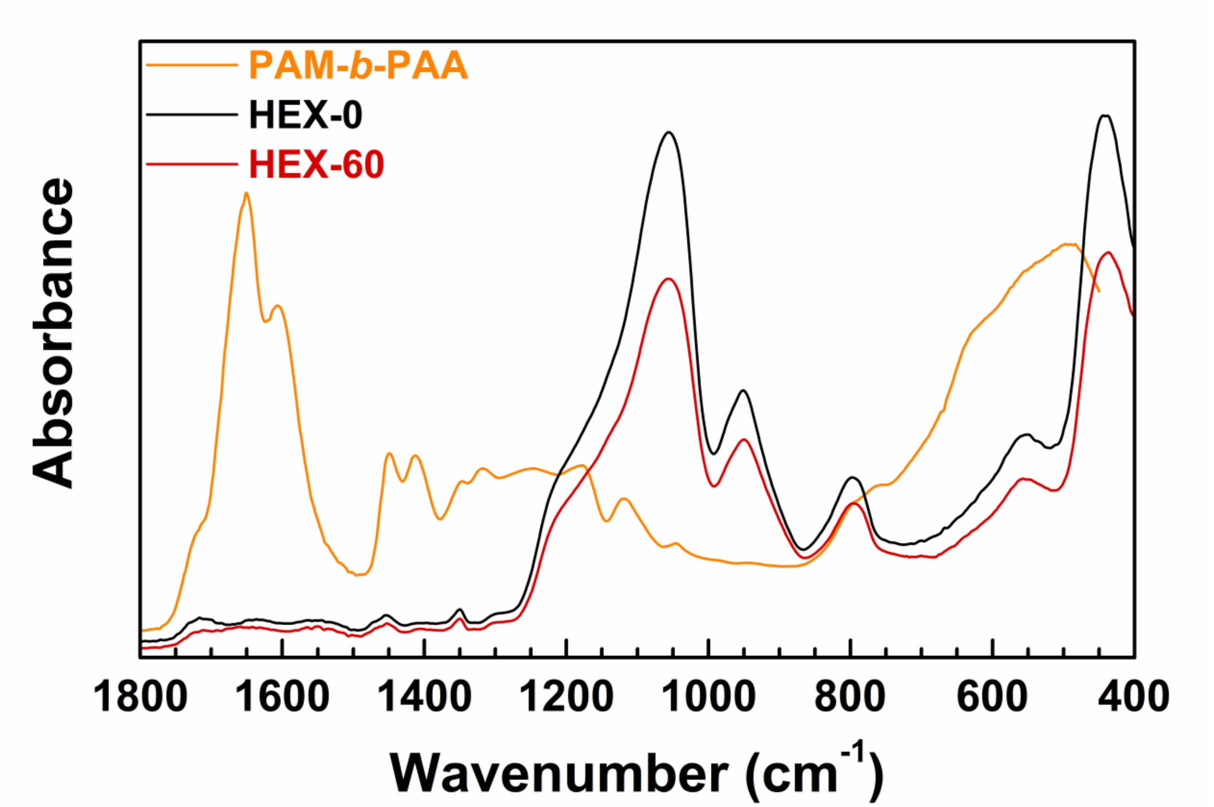

Fig. S3: ATR-FTIR spectra of HEX-0 and HEX-60 hybrid mesoPIC materials, and PAM-*b*-PAA copolymer.

S4. Supplementary N1S XPS spectra

We put into evidence the presence of PAM-*b*-PAA on the surface of hybrid particles by using a surface-specific analysis, ie. XPS. N$_{1S}$ XPS spectra of oligochitosan and PAM-*b*-PAA are presented on Fig. S4a. Two peaks were identified in the spectrum of oligochitosan: the NH$_2$ peak at 399.5 eV and NH$_3^+$ at 401.8 eV.[5,6] This assignment was verified by reacting oligochitosan with HCl or NaOH (Fig S4b). The amount of protonated NH$_3^+$ functions reaches up to 67% in acidic medium, while it was only 14% in basic medium, confirming the assignment. The PAM-*b*-PAA spectrum exhibits only one peak at 399.5 eV, assigned to N-C=O. The N$_{1S}$ spectra of **HEX-0** and **CUB-0** only present the two peaks of oligochitosan (56% of NH$_2$ and 44% of NH$_3^+$). The N$_{1S}$ spectrum of **HEX-60** required three peaks for fitting the curve: the NH$_2$ and NH$_3^+$ peaks of oligochitosan and the N-C=O amide peak related to PAM-*b*-PAA. Fitting of the curve was performed by fixing the position, width, and area ratio of the two peaks found for oligochitosan in **HEX-0** and **CUB-0**, and adjusting the parameters of the amide peak. The results of all the fittings, i.e. peak positions and peak areas, are listed in Table S4. For **HEX-60** particles, the peak area shows 35% of nitrogen of N-C=O amide type, which evidences the presence of PAM-*b*-PAA in significant amount on the outer surface of these particles. The **CUB-60** material exhibits only 11% of nitrogen of N-C=O amide type, indicating a smaller amount of PAM-*b*-PAA chains on the outer surface of particles compared to **HEX-60**.

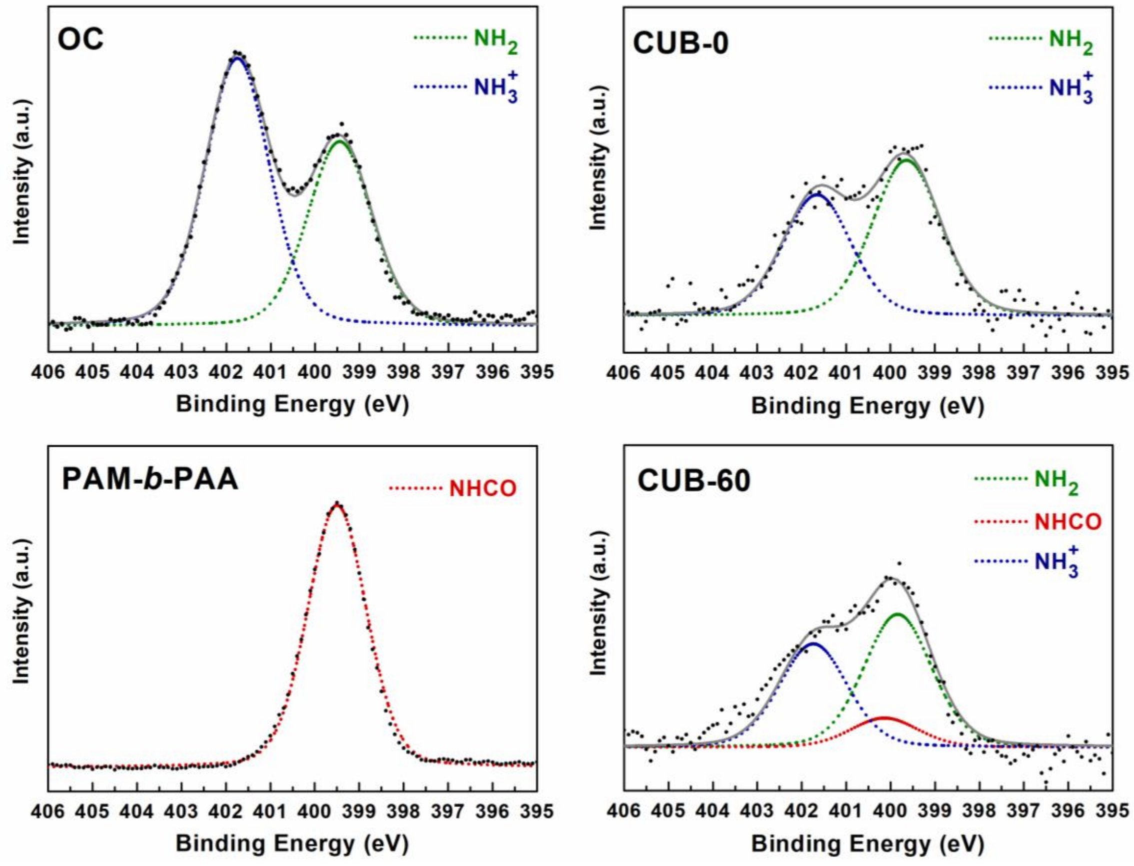

Fig. S4a. N$_{1s}$ XPS spectra of oligochitosan (OC), CUB-0, PAM-*b*-PAA and CUB-60

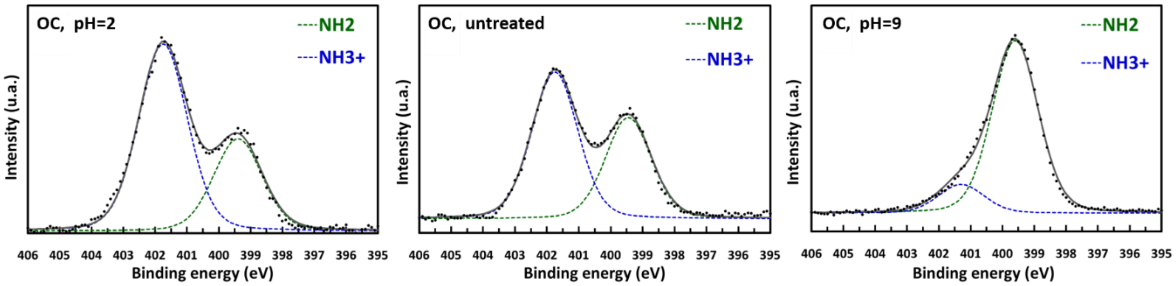

Fig. S4b: N_{1S} XPS spectra of oligochitosan treated at pH=2 (left), untreated (middle), and treated at pH=9 (right).

Table S4. Results from the curve fittings of the N_{1S} XPS spectra.

Sample	**NH_2**		**NH_3^+**		**NHCO**	
	Center (eV)	% Area	Center (eV)	% Area	Center (eV)	% Area
Oligochitosan	399.5	41%	401.8	59%	-	-
PAM-*b*-PAA	-	-	-	-	399.5	100%
HEX-0	399.6	56%	401.7	44%	-	-
HEX-60	399.6	37%	401.7	28%	399.9	35%
CUB-0	399.6	56%	401.7	44%	-	-
CUB-60	399.6	50%	401.7	39%	400.1	11%

S5. Influence of the synthesis process on the size of particles

The objective of this session is to vary the mixing degree of PAM-*b*-PAA and PEO-*b*-PAA within the PIC micelles. This was done by modifying the synthesis procedure in the case of a PAM-*b*-PAA/PEO-*b*-PAA weight ratio of 40/60, as for the synthesis of HEX-40 and CUB-40. The two different procedures used are schematically depicted in Fig. S5a. In the first procedure, called "mixed" process, two solutions were prepared separately, at pH 4.5, one containing TEOS only and the other a mixture of the structuring agent components: PEO-*b*-PAA, PAM-*b*-PAA and OC. The pH of each solution was adjusted at 4.5 before mixing the solutions together. In the second procedure, called "unmixed" process, two separate solutions containing on one side PEO-*b*-PAA/OC and on the other side PAM-*b*-PAA/OC with TEOS were prepared at pH = 4.5 before being mixed. Whatever the process, the final chemical composition of the synthesis medium was the same. By designing these two processes, we expected to enforce the formation of mixed PAM-*b*-PAA/PEO-*b*-PAA micelles ("mixed" process) to the detriment of singular micelles constituted by PAM-*b*-PAA or PEO-*b*-PAA ("unmixed" process). This should be a valuable method to evaluate the role of PAM-*b*-PAA in mixed corona PIC micelles in the formation of particles. TEM images of the materials obtained after calcination and nitrogen sorption isotherms with PSD are shown in Fig. S5b. They evidence a strong reduction in the particle size when PAM-*b*-PAA/PEO-*b*-PAA mixed micelles are formed at pH 4.5 before the introduction of the fast condensing silicic species; this highlights the crucial role of PAM-*b*-PAA in the PIC micelles with mixed corona for the formation of particles of controlled size.

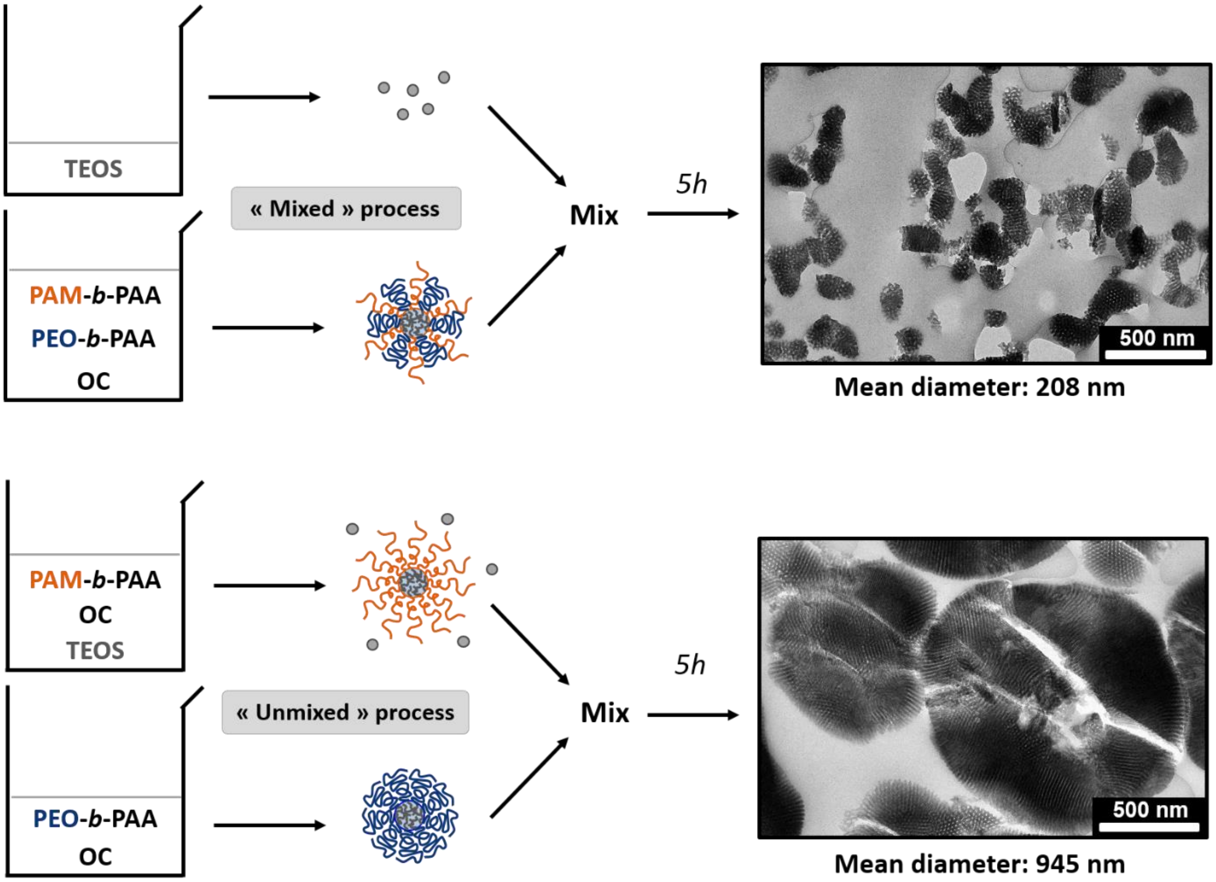

Fig. S5a: illustration of the different procedures (left) used to favor or not the mixing of the PAM and PEO chains in the corona of PIC micelles, and TEM images (right) of the resulting particles after microtome-cutting.

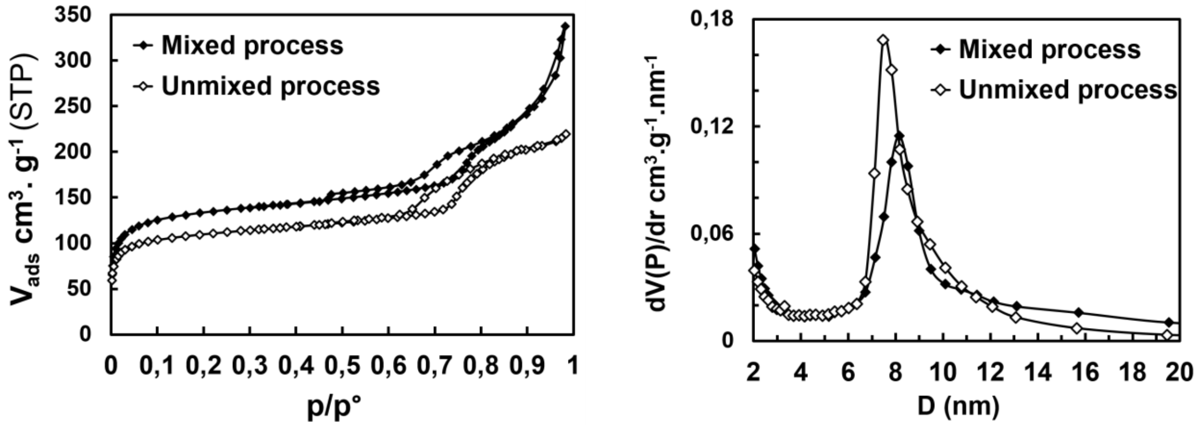

Fig. S5b: nitrogen sorption isotherms (left) and corresponding pore size distributions (right) of the calcined particles obtained using the "mixed" or "unmixed" process.

S6. Synthesis of HEX structure using PAPEO-*b*-PAA

S6.1. Synthesis

The synthesis described here aimed at preparing a material with a 2D HEX structure by using the comb-type PAPEO-*b*-PAA DHBC. The same comb-type block copolymer as the one used for the synthesis of the 3D cage-like structure has been used. The procedure followed for producing a 2D hexagonal mesostructure by using the PAPEO-*b*-PAA DHBC is similar to the preparation method yielding the 3D cage-like structure , which is described in section S1.3, except that: 1) an oligochitosan with a higher molecular weight of 7500 g.mol^{-1} (Creative PegWorks®) instead of the 2500 g.mol^{-1} was used, 2) the macroscopic precipitation was induced by raising the pH to 5.0 instead of 4.5. These changes were intended to decrease the interfacial curvature between the organic (PAA/OC) and inorganic (EO/Si) parts of the assembly that further defines the type of mesostructure.[7]

Small particles with stabilized surface were produced under these experimental conditions (OC of 7500 g.mol^{-1} and pH = 5 for the macroscopic precipitation) when replacing 40% of the PAPEO-*b*-PAA DHBC with PAM-*b*-PAA.

S6.2. Characterization

The textural characteristics of the particles are shown on Fig. S6. The nitrogen sorption isotherms of the calcined samples (Fig. S6a) strongly differ from $p/p^0 > 0.85$, indicating inter-particle porosity for the material synthesized in the presence of PAM-*b*-PAA. The SAXS patterns (Fig. S6b) and TEM images (Fig. S6c and d) confirm the long-range order of the 2D hexagonal structure in both materials.

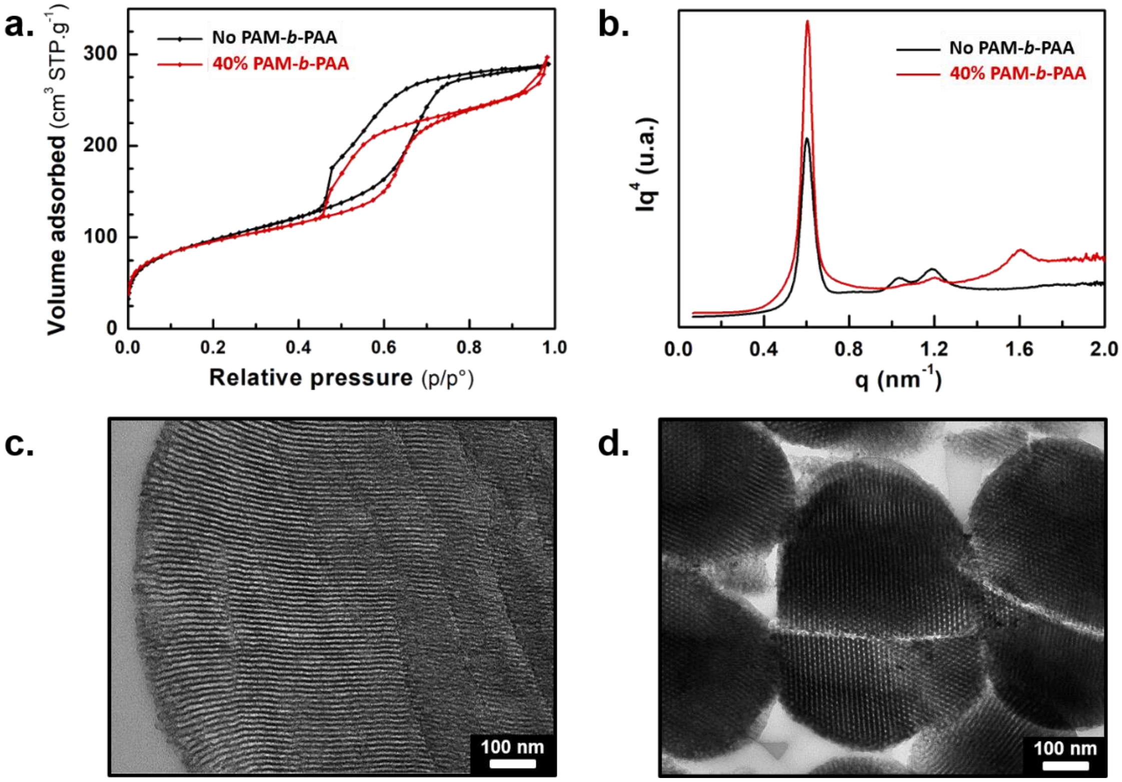

Fig S6: characteristics of the calcined 2D hexagonally structured particles synthesized using PAPEO-*b*-PAA, in the absence and presence of 40% PAM-*b*-PAA. a) nitrogen sorption isotherms, b) SAXS patterns, c) TEM image of microtome-cut particles synthesized in the absence of PAM-*b*-PAA, d) TEM image of particles synthesized in the presence of 40% PAM-*b*-PAA.

S7. Influence of the PAM-*b*-PAA chain length on the size of particles

The influence of the length of the PAM chain in PAM-*b*-PAA on the size of the particles was studied by replacing one PAM_{140}-*b*-PAA_{40} chain with two PAM_{70}-*b*-PAA_{20} chains, so that the overall numbers of AA and AM units remain the same in the synthesis medium while the length of both blocks was divided by two. Under such conditions, the amounts of PAM-*b*-PAA, PEO-*b*-PAA and TEOS in the synthesis medium were unchanged. The TEM images of the calcined particles obtained are shown in Fig. S7a and the particle size distributions in Fig. S7b. Shortening the polymer significantly increases the size of particles from 302 nm to 473 nm and broadens the size distribution.

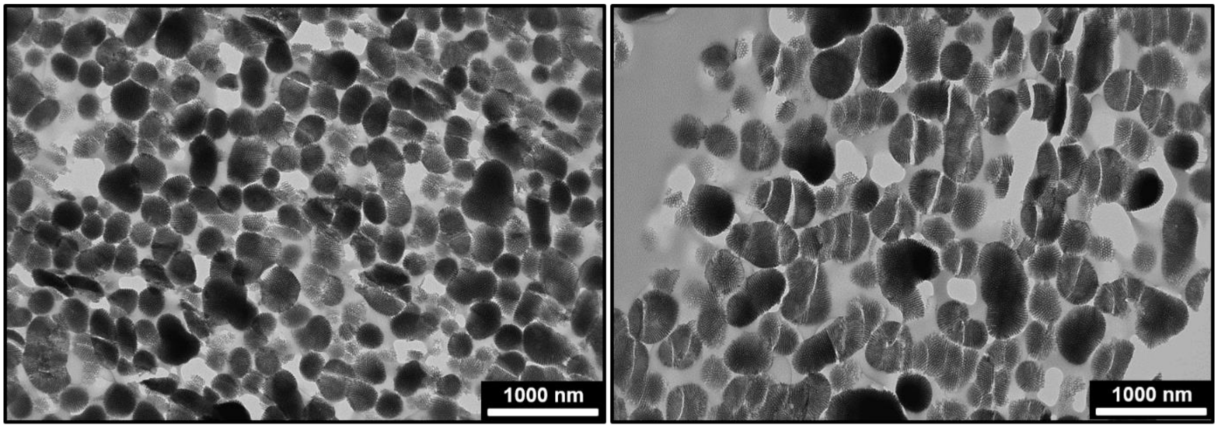

Fig. S7a: TEM images of microtome-cut calcined particles synthesized using PAM_{140}-*b*-PAA_{40} (left), and PAM_{70}-*b*-PAA_{20} (right).

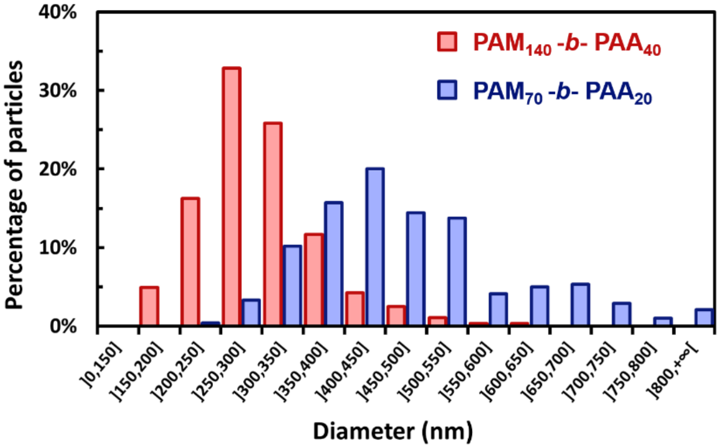

Fig. S7b: Distribution of particle diameters of materials synthesized using 40% of PAM-*b*-PAA of different molecular weights. (n>300).

S8. Formation of lamellar mesoPIC particles

S8.1. Synthesis

Particles exhibiting a lamellar mesostructure were obtained using a procedure similar to that described in section S1.3, which was used to produce 2D hexagonal materials with PEO-*b*-PAA, except that: 1) an oligochitosan with a larger molecular weight of 7500 g.mol^{-1} (Creative PegWorks®) instead of the 2500 g.mol^{-1} was used, 2) macroscopic precipitation was induced by raising the pH to 5.5 instead of 4.5. These changes were intended to decrease the interfacial curvature between the organic (PAA/OC) and inorganic (EO/Si) parts of the assembly that further defines the type of mesostructure.[7] **LAM-0** was synthesized without PAM-*b*-PAA while **LAM-40** was synthesized by replacing 40% of the PEO-*b*-PAA DHBC with PAM-*b*-PAA.

S8.2. Characterization

The textural characteristics of **LAM-0** and **LAM-40** are shown on Fig. S7. The nitrogen sorption isotherms of the calcined samples (Fig. S8a) strongly differ from $p/p^0 > 0.85$, where the porosity observed for **LAM-40** is due to inter-particle voids. SAXS patterns (Fig. S8b) and TEM images (Fig. S8c and d) confirm the long-range order of the lamellar structure of both materials.

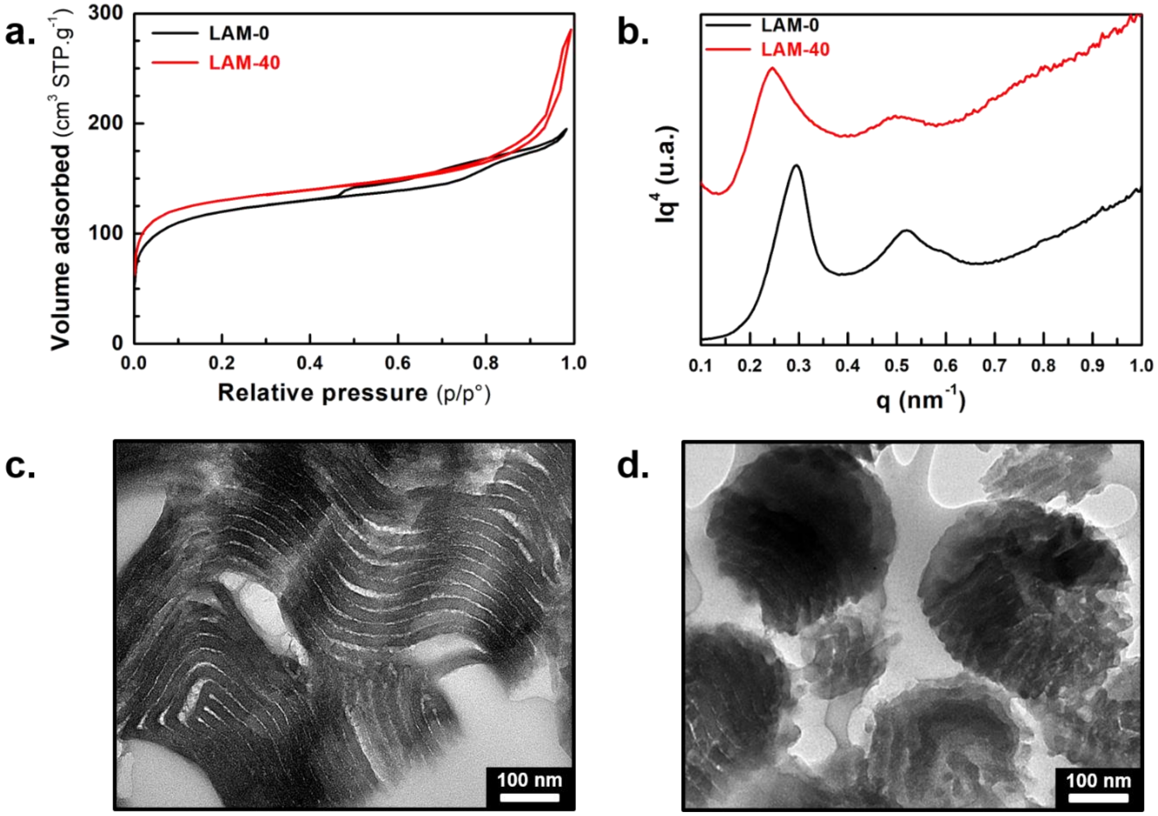

Fig S8: characteristics of LAM-0 and LAM-40. a) nitrogen sorption isotherms after calcination, b) SAXS patterns of the hybrid particles, c) TEM image of a hybrid microtome-cut LAM-0 particle, d) TEM image of hybrid microtome-cut LAM-40 particles.

S9. Characterization of DHBC polymers

S9.1 PEO-*b*-PAA

- **PEO$_{227}$-CTA**

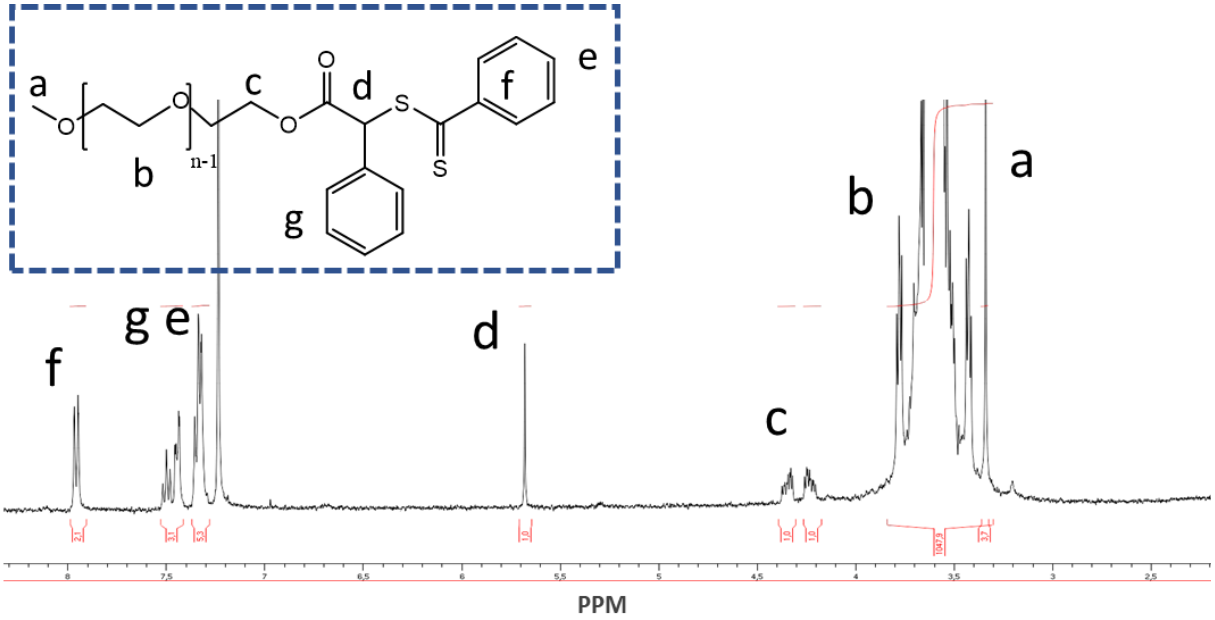

Figure S9.1.a ^{1}H NMR (400MHz, Bruker) spectrum of PEO$_{227}$-CTA in CDCl$_3$.

- **PEO$_{227}$-*b*-PAA$_{40}$**

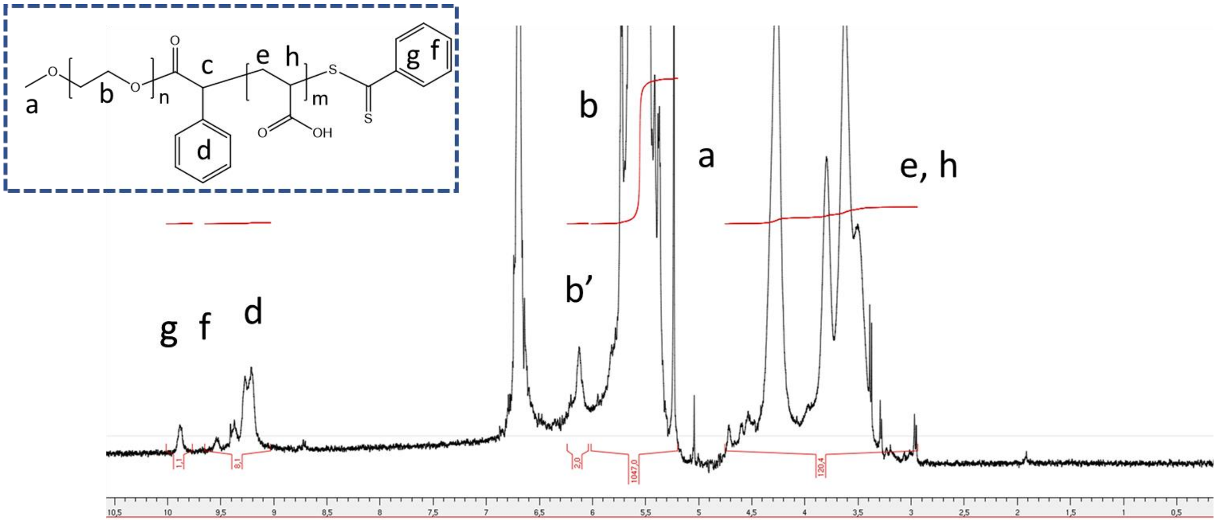

Figure S9.1.b ^{1}H NMR (400MHz, Bruker) spectrum of PEO$_{227}$-*b*-PAA$_{40}$ in D$_2$O.

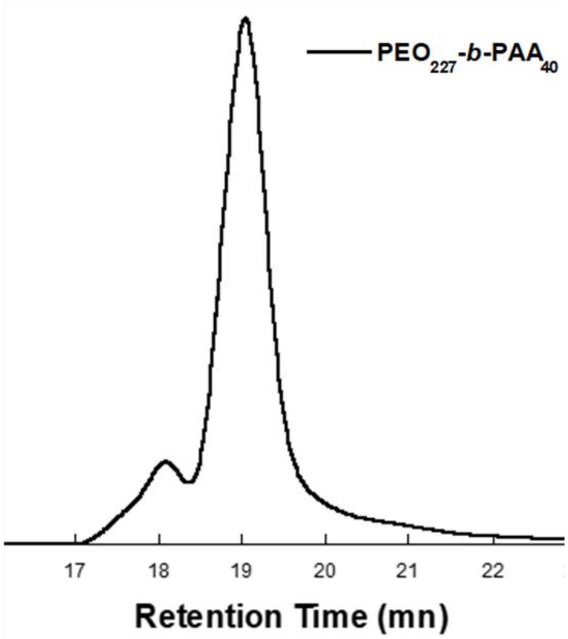

Figure S9.1.c Characterization of PEO-*b*-PAA by SEC-DMF after methylation of PAA with trimethylsilyl diazomethane. A molar mass in number Mn = 16 526 g.mol^{-1} was determined with calibration with PMMA standards. Typical sample concentration at 10 mg.mL^{-1}. Solvent: DMF with 0.1 wt.% of LiBr as eluant and toluene as flux marker, flow: 0.8 mL.min^{-1}. System Agilent technology: two columns PL1113-6300 resipore 300 * 7.5 mm and three detectors: refractive index PL0390-0601, two angles 15° and 90° light scattering and capillary viscometer PL0390-06034.

S9.2 PAPEO-*b*-PAA

- **PAA$_{45}$-CTA**

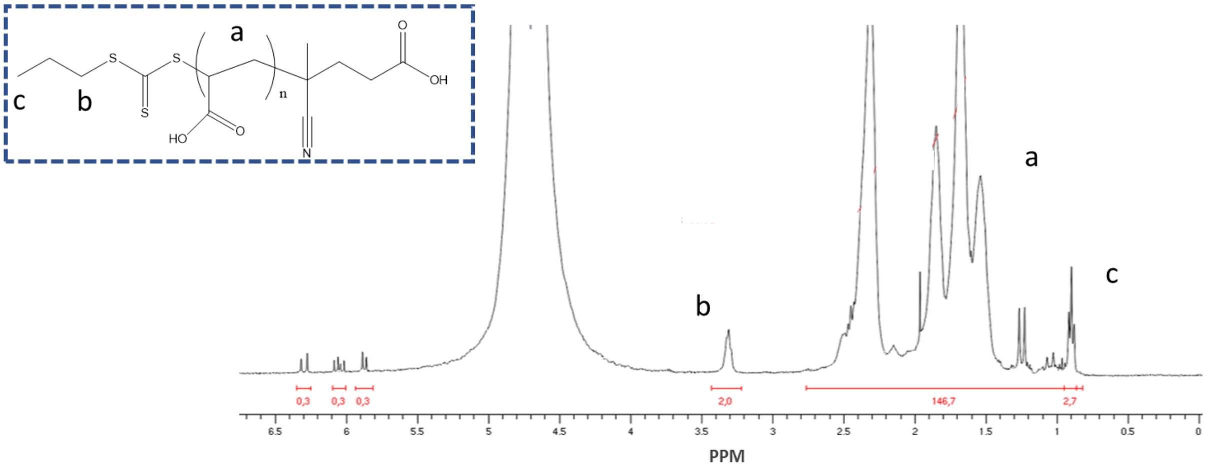

Figure S9.2.a ^{1}H NMR (400MHz, Bruker) spectrum of PAA$_{45}$-CTA in D$_2$O.

- **PAA_{45}-*b*-$PAPEO_{22}$-CTA**

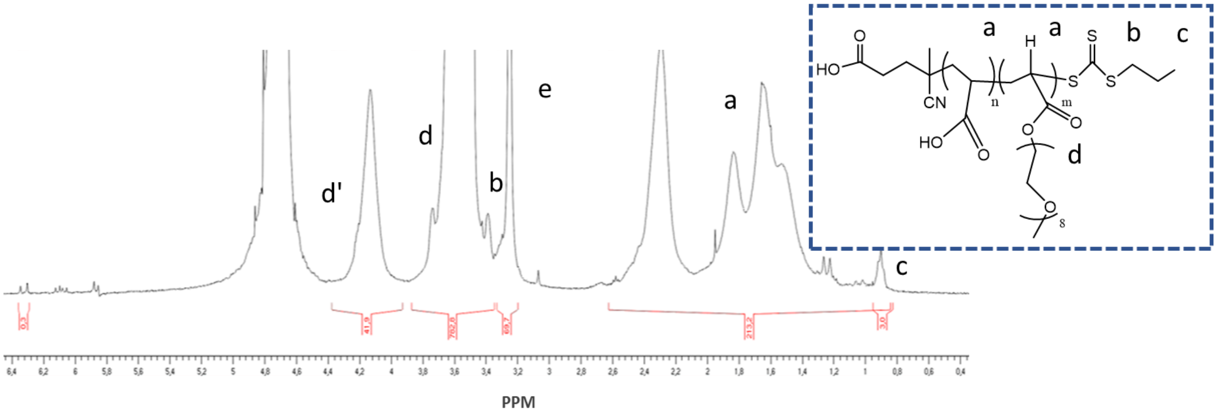

Figure S9.2.b ^{1}H NMR (400MHz, Bruker) spectrum of PAA_{45}-*b*-$PAPEO_{22}$ in D_2O.

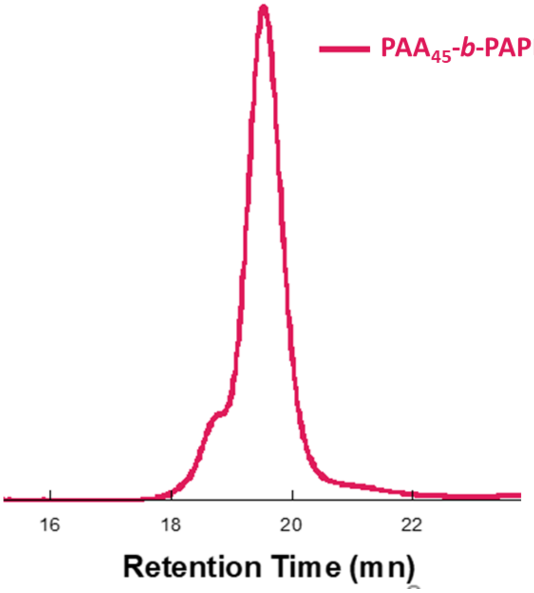

Figure S9.2.c Characterization of PAPEO-*b*-PAA by SEC-DMF after methylation of PAA with trimethylsilyl diazomethane. A molar mass in number Mn = 11 865 $g.mol^{-1}$ was determined with calibration with PMMA standards. Typical sample concentration at 10 $mg.mL^{-1}$. Solvent: DMF with 0.1 wt.% of LiBr as eluant and toluene as flux marker, flow: 0.8 $mL.min^{-1}$. System Agilent technology: two columns PL1113-6300 resipore 300 * 7.5 mm and three detectors: refractive index PL0390-0601, two angles 15° and 90° light scattering and capillary viscometer PL0390-06034.

S9.3 PAM-*b*-PAA

- **PAM140-Xa**

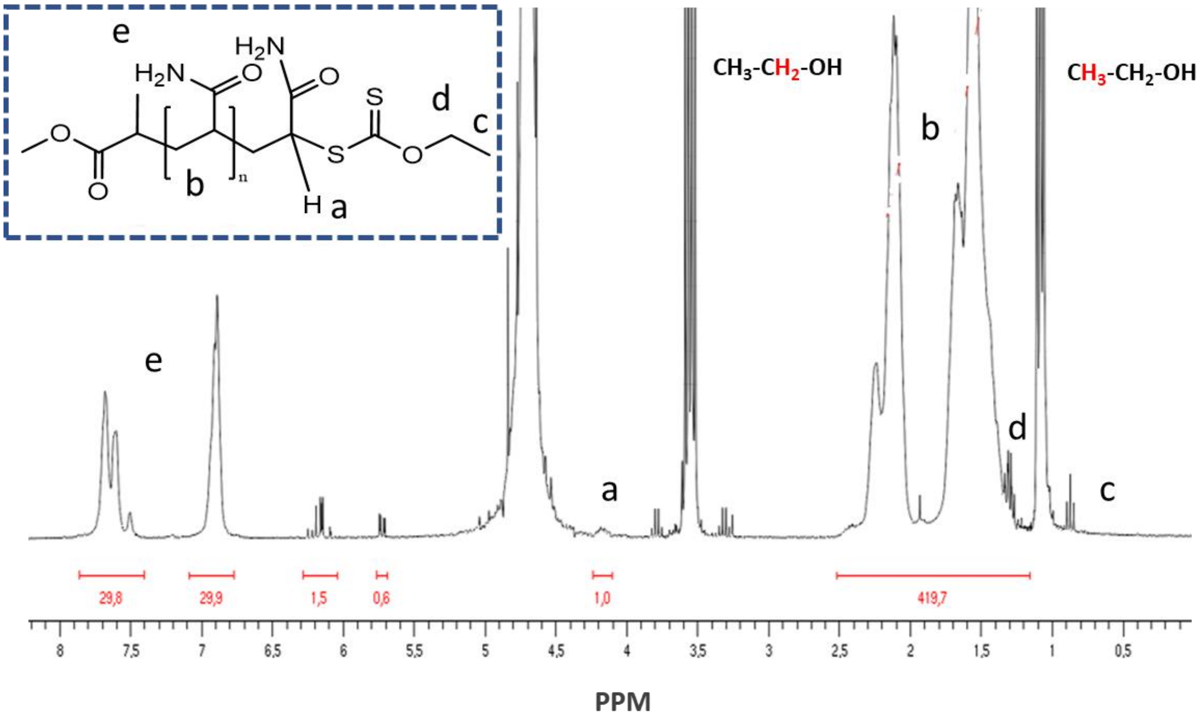

Figure S9.3.a ^{1}H NMR (400MHz, Bruker) spectrum of PAM-Xanthate macro-CTA in D_2O (with ethanol and water traces).

- **PAM$_{140}$-*b*-PAA$_{40}$-Xa**

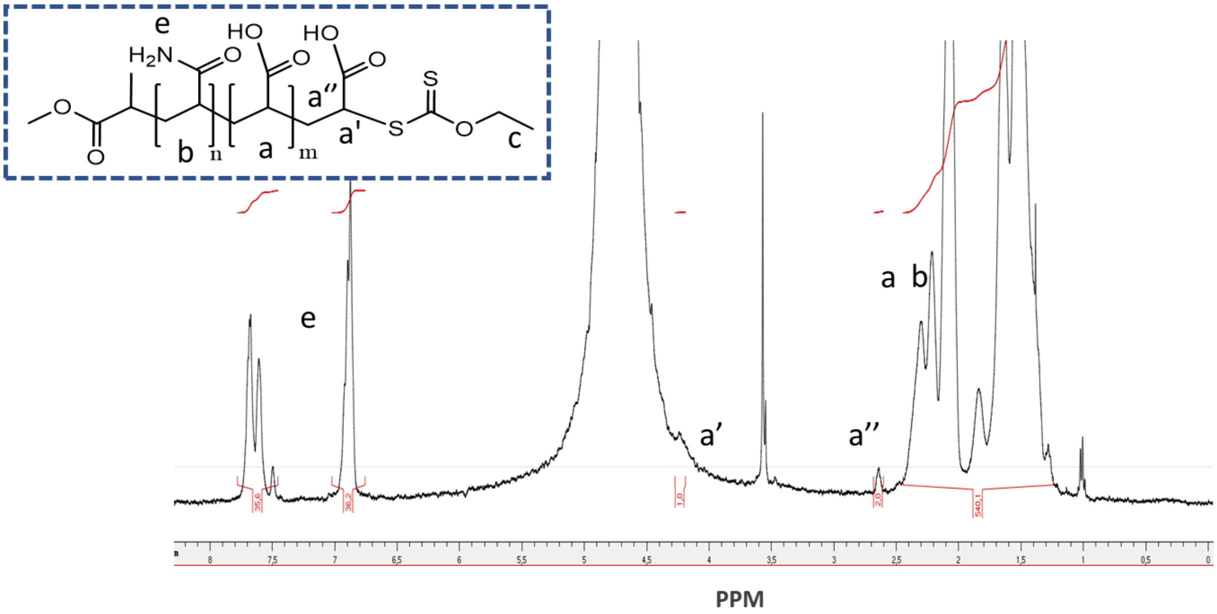

Figure S9.3.b ^{1}H NMR (400MHz, Bruker) spectrum of PAM$_{140}$-*b*-PAA$_{40}$-Xa in D$_2$O.

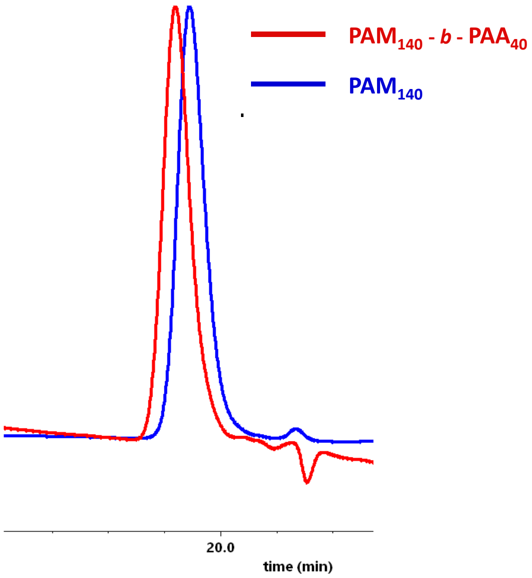

Figure S9.3.c PAM-*b*-PAA characterization by aqueous-SEC, determination of molecular weight by laser light scattering. Typical samples concentration is at 10 mg.ml^{-1}. Solvent is an aqueous buffer solution at pH = 7 with [NaH$_2$PO$_4$] = 0.15 M and adjust with HCl, [NaNO$_3$] = 0.1 M and [NaN$_3$] = 100 ppm, the solution is filtrated with Durapore 0.10 µm filter prior to utilization. A guard column SHODEX OHpak SBG (50 X 6 mm) and two columns SHODEX SB-806M-HQ (300 X 8 mm) in series were used. Polymers were detected using laser light scattering detectors at 690 nm (Wyatt Technology) with 3 angles of detections (45°, 90° and 135°) and a refractometer RID-6A (Shimadzu). The system is thermostated at 35 °C.